

”Journal of Computational Neuroscience”, in press.

Thermodynamic constraints on neural dimensions, firing rates, brain temperature and size

Jan Karbowski

*Sloan-Swartz Center for Theoretical Neurobiology, Division of Biology 216-76,
California Institute of Technology, Pasadena, CA 91125, USA;
Institute of Biocybernetics and Biomedical Engineering,
Polish Academy of Sciences, 02-109 Warsaw, Poland*

Email: jkarb@its.caltech.edu

Abstract

There have been suggestions that heat caused by cerebral metabolic activity may constrain mammalian brain evolution, architecture, and function. This article investigates physical limits on brain wiring and corresponding changes in brain temperature that are imposed by thermodynamics of heat balance determined mainly by Na^+/K^+ -ATPase, cerebral blood flow, and heat conduction. It is found that even moderate firing rates cause significant intracellular Na^+ build-up, and the ATP consumption rate associated with pumping out these ions grows nonlinearly with frequency. Surprisingly, the power dissipated by the Na^+/K^+ pump depends biphasically on frequency, which can lead to the biphasic dependence of brain temperature on frequency as well. Both the total power of sodium pumps and brain temperature diverge for very small fiber diameters, indicating that too thin fibers are not beneficial for thermal balance. For very small brains blood flow is not a sufficient cooling mechanism deep in the brain. The theoretical lower bound on fiber diameter above which brain temperature is in the operational regime is strongly frequency dependent but finite due to synaptic depression. For normal neurophysiological conditions this bound is at least an order of magnitude smaller than average values of empirical fiber diameters, suggesting that neuroanatomy of the mammalian brains operates in the thermodynamically safe regime. Analytical formulas presented can be used to estimate average firing rates in mammals, and relate their changes to changes in brain temperature, which can have important practical applications. In general, activity in larger brains is found to be slower than in smaller brains.

Keywords: Metabolism; Heat balance; Brain size; Fiber diameter; Temperature; Wiring; Limits.

1 Introduction

Brain like any computational device (Landauer 1961; Bennett, 1982) or biological organ (Rolfe and Brown, 1997) dissipates energy (Siesjo, 1978; Ames, 2000; Clarke and Sokoloff, 1994). Recent studies on cerebral metabolism indicate that brain is energy expensive (Aiello and Wheeler, 1995; Attwell and Laughlin, 2001; Lennie, 2003), as it consumes relatively more energy than most other organs, and its total metabolic rate has larger scaling exponent than whole body metabolic rate (Karbowski, 2007). Potential thermal imbalance between heat produced and removed could lead to overheating and aberrant functioning, because neural properties are strongly temperature dependent (Koch, 1998). Therefore, the problem of heat transfer could be a serious factor shaping brain evolution (Falk, 1990), organization, and function (Baker, 1982; Raichle, 2003; Kiyatkin, 2007). Consequently, what is the relationship between brain temperature, its size, cerebral power generated and neural activity? Can we estimate changes in firing rates based on changes in temperature? Is there any thermodynamic limit on brain size? If so, does 5 kg, which is the mass of the largest mammalian brain (Haug, 1987; Purves, 1988), approach that limit? Are neural sizes and fibers also constrained by thermodynamics, and if so to what extent? How fast can neural computation be to maintain thermal balance and physiological range of intracellular ionic concentrations?

This article answers these questions by finding the power generated by sodium metabolic pumps and relating this power to the thermal and neuroanatomical properties of brain tissue. From this, we determine theoretical thermal bounds on fiber dimensions, and compare them with empirical data. These bounds enable us to esti-

mate the upper theoretical limits on the density of brain wiring.

2 Methods

2.1 Voltage and Na⁺-K⁺ dynamics.

Na⁺ and K⁺ are two major ions affecting neural membrane dynamics (Kandel et al, 1991; Koch, 1998) and its energetics (Astrup et al, 1981; Erecinska and Silver, 1989; Rolfe and Brown, 1997; Ames, 2000). The energy consuming Na⁺/K⁺ pump affects membrane electrical properties, because it pumps out 3 Na⁺ and pumps in 2 K⁺ per 1 ATP molecule consumed (Kandel et al, 1991). The equations governing membrane and Na⁺/K⁺-ATP activities of a neuron are given by:

$$\begin{aligned}
 CS \frac{dV}{dt} &= -g_{Na}S(V - V_{Na}) - g_KS(V - V_K) - g_LS(V - V_L) - I_p - I_s, \\
 U_nF \frac{d[\text{Na}]}{dt} &= -g_{Na}S(V - V_{Na}) - 3I_p - \alpha I_s, \\
 U_nF \frac{d[\text{K}]}{dt} &= -g_KS(V - V_K) + 2I_p - \beta I_s,
 \end{aligned}
 \tag{1}$$

where V is the membrane potential, C is the membrane capacitance per unit area, S is neuron's membrane surface area (primary axons and dendrites), V_{Na} and V_K are

Na⁺ and K⁺ reversal potentials, g_{Na} and g_K are voltage-dependent Na⁺ and K⁺ conductances per unit membrane area, g_L is the leak conductance and V_L is the reversal potential corresponding to the leak current. The parameter U_n denotes neuron's volume, F is the Faraday constant. The current I_p is the Na⁺/K⁺ pump current given by $I_p = AS[\text{Na}]^k/([\text{Na}]^k + \theta^k)$ where $\theta = 20.0$ mM, A is the maximal pump current per membrane surface area, and k is the Hill constant. The symbol [...] denotes intracellular ionic concentration, I_s is the synaptic current, and α , β are voltage dependent proportionality parameters determined below.

Voltage dependent conductances are represented by $g_{Na} = m^3 h \bar{g}_{Na}$ and $g_K = n^4 \bar{g}_K$, where \bar{g}_{Na} and \bar{g}_K are the maximal Na⁺ and K⁺ conductances. The gating variables h and n obey the standard kinetic equation $dx/dt = \alpha_x(1 - x) - \beta_x x$, (for $x = h, n$), and the fast variable m is set to its equilibrium value $\alpha_m/(\alpha_m + \beta_m)$. Voltage dependences of the parameters α_x and β_x were chosen, with a slight modification, as in the Traub-Miles model (1991), which describes a pyramidal neuron in the hippocampus. Specifically, for sodium channels: $\alpha_m = 0.32(V + 54)/(1 - \exp(-(V + 54)/4))$, $\beta_m = 0.28(V + 27)/(\exp((V + 27)/5) - 1)$, $\alpha_h = 0.128 \exp(-(V + 50)/18)$, $\beta_h = 4.0/(1 + \exp(-(V + 27)/5))$, and for potassium channels $\alpha_n = 0.044(V + 52)/(1 - \exp(-(V + 52)/5))$, $\beta_n = 0.5 \exp(-(V + 57)/40)$, where V is expressed in mV.

It is assumed that the neuron represented by Eq. (1) is embedded in the network of neurons firing with an average firing rate f . The synaptic current of a single synapse is $qg_s e^{-t/\tau_s}(V - V_s)$, where q is the release probability, g_s is the maximal synaptic conductance (it is assumed that the rising phase of synaptic conductance is much faster

that its decaying phase that is characterized by the time constant τ_s), and V_s is the reversal potential for synapses. Since the majority of synapses in the mammalian brain are excitatory and glutamate (Braitenberg and Schuz, 1998), we have $V_s = 0$ (Koch, 1998). The average synaptic conductance is $f \int_0^{1/f} dt qg_s e^{-t/\tau_s}$, which in the physiologically valid limit $f\tau_s \ll 1$ yields $qg_s f\tau_s$. Neurophysiological data indicate (Markram et al, 1997) that the release probability q is frequency dependent. Here, we follow Dayan and Abbott (2001) and assume that synaptic depression modifies the release probability according to $q(f) = q_0/(1 + \gamma\tau_d f)$, where q_0 is the release probability at 0 Hz, τ_d is the depression time constant, and γ is the parameter controlling the degree of depression (for $\gamma = 0$ lack of depression, for $\gamma = 1$ maximal depression). Thus, the total average synaptic current is $I_s = f q_0 M g_s \tau_s (V - V_s)/(1 + \gamma\tau_d f)$, where M is the number of synapses (or presynaptic neurons) per neuron. Fluctuations around the average I_s cause the neuron to fire an action potential with an average firing rate f . Glutamate synapses with non-NMDA receptors are used more frequently for regular transmission (NMDA receptors are blocked by Mg^{2+} ; Kandel et al, 1991) and therefore only these are considered here. Synaptic current of non-NMDA type is composed almost exclusively of Na^+ and K^+ ions, which is the reason for the presence of αI_s and βI_s terms in the dynamics of $[Na]$ and $[K]$ in Eq. (1), where $\alpha + \beta = 1$.

The parameter α can be determined in a few steps. First, we can write the synaptic current I_s as $I_s = \tilde{g}_{Na}(V - V_{Na}) + \tilde{g}_K(V - V_K)$, where \tilde{g}_K and \tilde{g}_{Na} are K^+ and Na^+ conductances (voltage independent) at glutamatergic synapses. Since for $V = V_s = 0$ the synaptic current $I_s = 0$, we have $\tilde{g}_K = -\tilde{g}_{Na}V_{Na}/V_K$. Second, from the condition

$\alpha I_s = \tilde{g}_{Na}(V - V_{Na})$, we obtain $\alpha = \tilde{g}_{Na}(V - V_{Na})/(\tilde{g}_{Na}(V - V_{Na}) + \tilde{g}_K(V - V_K))$, which leads to $\alpha = V_K(V - V_{Na})/\{V(V_K - V_{Na})\}$. Note that α is voltage dependent. Consequently, the synaptic contribution to changes in intracellular Na^+ concentration is given by $\alpha I_s = q(f) f M g_s \tau_s (V - V_{Na}) V_K / (V_K - V_{Na})$. The synaptic contribution to changes in intracellular K^+ is $\beta I_s = -q(f) f M g_s \tau_s (V - V_K) V_{Na} / (V_K - V_{Na})$.

Equation for voltage dynamics in Eq. (1) assumes that the membrane is equipotential, i.e., axons and dendrites have on average equal potentials. This assumption neglects spatio-temporal effects associated with action potential propagation. The validity of this approximation is discussed in the Discussion section and in Appendix A.

Adding appropriately sides in Eq. (1) we obtain the ‘‘charge conservation’’ equation:

$$U_n F \frac{d}{dt} ([Na] + [K]) = C S \frac{dV}{dt} + g_L (V - V_L). \quad (2)$$

This equation reflects the fact that non-zero membrane potential is caused by concentration gradients of charged ions across membrane, and temporal changes in potential are directly related to the temporal changes in ionic concentrations. This temporal relationship during an initial phase of an action potential is discussed in the Results section. Here, we focus instead on the long-term relation between intracellular $[\text{Na}]$ and $[\text{K}]$. In this regime and for firing rates < 100 Hz (duration of action potential and voltage recovery $\sim 10 - 15$ msec), the average of V is close to its resting potential V_o , which in turn is very close to V_L . Thus, on the long-time scale, the right hand side of

Eq. (2) is close to 0, which implies that $[\text{Na}] + [\text{K}] \approx \text{const}$. That is, changes in $[\text{Na}]$ directly determine changes in $[\text{K}]$, and practically there is no need to solve the equation for the potassium dynamics. Values of neurophysiological parameters used in this paper are presented in Table 1.

2.2 Neuroanatomical relationships.

In studying metabolic and thermodynamic properties of brain tissue the following neuroanatomical relations were used: (i) volume density of synapses $\rho_s = NM/U_g$ is brain size independent, where N is the number of neurons and U_g is the cortical gray matter volume (Braitenberg and Schuz, 1998; DeFelipe et al, 2002); (ii) the fraction $1 - \phi$ of the gray matter volume taken by fibers (axons and dendrites) is approximately constant and about 2/3 (Braitenberg and Schuz, 1998); (iii) white matter volume U_w scales with gray matter volume U_g as $U_w = 0.166U_g^{1.23}$ (Zhang and Sejnowski, 2000), where U_g and U_w are expressed in cm^3 .

The relationship between neuron's surface area S and gray matter volume U_g can be determined as follows. The gray matter volume is $U_g = NU_n + \phi U_g$, where neuron's volume $U_n = (l_a d_a^2 + l_d d_d^2)\pi/4$ with l_a, l_d denoting average (unmyelinated) axon and dendrite length in the gray matter and d_a, d_d denoting their corresponding diameters (neuron's soma is neglected as it is small). The parameter ϕ is the fraction of volume taken by non-fibers (synapses, blood vessels, etc). The neuron's surface area is $S = \pi(l_a d_a + l_d d_d)$. We define "an effective" fiber diameter d as

$$d \equiv (l_a d_a^2 + l_d d_d^2)/(l_a d_a + l_d d_d), \quad (3)$$

which is proportional to the neuron's volume to surface ratio, i.e., $d = 4U_n/S$. In fact, if volumes of axons and dendrites are equal, which seems to be neuroanatomically valid in the gray matter (Braitenberg and Schüz, 1998; Chklovskii et al, 2002), then d represents a harmonic mean of axonal d_a and dendritic d_d diameters, that is $d = 2d_a d_d / (d_a + d_d)$. This formula can be derived by noting that axon length $l_a = l_d (d_d / d_a)^2$ (equal volumes of axons and dendrites), and substituting l_a to Eq. (3). Note that for constant d_d , the effective diameter d decreases with decreasing d_a . In the limit $d_a / d_d \ll 1$, we have $d \approx 2d_a$.

For neuroanatomical values of $d_a = 0.3 \mu\text{m}$ and $d_d = 0.9 \mu\text{m}$ in mouse (Braitenberg and Schüz, 1998), we obtain the effective fiber diameter $d = 0.45 \mu\text{m}$. Since the average values of cortical axon and dendrite diameters are roughly invariant with respect to brain size (i.e., they should be more or less the same for mouse and human; Braitenberg and Schüz, 1998), we can expect that the effective fiber diameter d should not change with brain size either. Therefore, we will use the above value of $d = 0.45 \mu\text{m}$ for illustrative purposes throughout the paper. Apart from that, occasionally we will also show results for the smallest experimentally known axons of diameter $0.1 \mu\text{m}$ corresponding to $d = 0.18 \mu\text{m}$ (for $d_d = 0.9 \mu\text{m}$), and for the smallest molecularly feasible axons (neurites) of diameter $0.06 \mu\text{m}$ (axons without Sodium channels that lack action potentials; Faisal et al, 2005), corresponding to $d = 0.11 \mu\text{m}$ (also for $d_d = 0.9 \mu\text{m}$).

With the definition of d we can relate the total surface area of neurons, NS , to the gray matter volume U_g as

$$NS = 4(1 - \phi)U_g/d, \quad (4)$$

and relate the surface density of synapses along axons and dendrites, M/S , to synaptic density ρ_s as

$$\frac{M}{S} = \frac{\rho_s d}{4(1 - \phi)}. \quad (5)$$

These relations are used below to rewrite Eq. (1) in a more convenient form for numerical and analytical calculations.

2.3 Explicit voltage and ionic dynamics.

With the modifications and interdependencies between parameters described in Subsections 2.1 and 2.2 we can rewrite Eq. (1) as:

$$\begin{aligned} C \frac{dV}{dt} &= -g_{Na}(V - V_{Na}) - g_K(V - V_K) - g_L(V - V_L) \\ &\quad - \frac{A[\text{Na}]^k}{[\text{Na}]^k + \theta^k} - \frac{q(f)f\rho_s dg_s \tau_s V}{4(1 - \phi)} + \text{synaptic fluct.} \\ \frac{dF}{4} \frac{d[\text{Na}]}{dt} &= - \left(g_{Na} + \frac{q(f)f\rho_s dg_s \tau_s V_K}{4(1 - \phi)(V_K - V_{Na})} \right) (V - V_{Na}) - \frac{3A[\text{Na}]^k}{[\text{Na}]^k + \theta^k} \\ \frac{dF}{4} \frac{d[\text{K}]}{dt} &= - \left(g_K - \frac{q(f)f\rho_s dg_s \tau_s V_{Na}}{4(1 - \phi)(V_K - V_{Na})} \right) (V - V_K) + \frac{2A[\text{Na}]^k}{[\text{Na}]^k + \theta^k}, \end{aligned} \quad (6)$$

where the release probability modulated by synaptic depression is $q(f) = q_0/(1 + \gamma\tau_d f)$

(Dayan and Abbott, 2001). These equations are solved both numerically (using the 4th-order Runge-Kutta method) and approximately analytically. Fast synaptic fluctuations denoted symbolically in the top equation of Eq. (6) cause the neuron to fire stochastically with the average frequency f (i.e. on average, every $1/f$ seconds the voltage is set to -20 mV).

2.4 Electric power generated by Na^+/K^+ -ATP pumps.

Since the metabolic rate in white matter is 3-4 times lower than in gray matter (Siesjo, 1978; Karbowski, 2007), the white matter contribution to the total brain metabolic power is neglected. The average power P_{ATP} dissipated by N neurons in the gray matter is given by

$$P_{ATP} = \frac{N}{\Delta t} \int_0^{\Delta t} dt (-3I_p(V - V_{Na}) + 2I_p(V - V_K)), \quad (7)$$

where the integral represents the electrical work performed by Na^+/K^+ -ATP pumps during the long time Δt , much larger than the average interspike interval $1/f$. This work goes for removing 3 Na^+ ions and importing 2 K^+ ions against their electrochemical gradients, which cost 1 ATP molecule (Kandel et al, 1991). Opposite signs in front of $3I_p$ and $2I_p$ indicate the fact that Na^+ and K^+ ions move in opposite directions through the membrane.

Integral in Eq. (7) can be estimated by noting that in the long-time limit the pump current I_p assumes its average value (with some fluctuations around, see the Results)

given by $I_{p,av} = AS[\text{Na}]_{av}^k / ([\text{Na}]_{av}^k + \theta^k)$, where $[\text{Na}]_{av}$ is the average long-term sodium concentration (determined in the Results section). In this limit, the average value of voltage $V(t)$ is approximately equal to its resting value V_o . Thus, the electric power P_{ATP} is

$$P_{ATP} \approx \frac{NSA[\text{Na}]_{av}^k}{([\text{Na}]_{av}^k + \theta^k)} (3V_{Na} - 2V_K - V_o), \quad (8)$$

where $V_{Na} = (RT/F) \ln([\text{Na}]_{ex}/[\text{Na}]_{av})$ and $V_K = (RT/F) \ln([\text{K}]_{ex}/[\text{K}]_{av})$, with the extracellular Na^+ and K^+ concentrations (Hille, 2001): $[\text{Na}]_{ex} = 145$ mM, and $[\text{K}]_{ex} = 4$ mM.

2.5 Mechanisms of brain cooling.

The major contribution to the cerebral metabolic rate or heat constitute Na^+/K^+ -ATPase (Astrup et al, 1981; Erecinska and Silver, 1989; Rolfe and Brown, 1997; Ames, 2000). Therefore, in this paper, the heat coming from other reactions such as glycolysis (conversion of glucose to ATP) is assumed to be less important and hence it is neglected in the estimates. In deep brain regions heat generated by hydrolysis of ATP molecules and coupled to it activity of Na^+/K^+ pumps is transferred by conduction and circulating cerebral blood flow, whereas at the surface (scalp) the heat is removed mostly by convection/conduction and radiation (Fig. 1). Heat conduction (convection) is associated with the existence of a temperature gradient between the brain or scalp and the external environment. Heat radiation is a quantum mechanical property of every physical object

having temperature above absolute zero. Transfer of heat to the circulating cerebral blood in deep brain regions is possible because incoming blood (artery) has a slightly lower temperature than the brain tissue in this region (Hayward and Baker, 1968; Nybo et al, 2002; Kiyatkin, 2007). In general, the incoming blood temperature corresponds to the core body temperature, which is assumed to be a constant because it changes on time scales that are much slower than changes in brain temperature (Kiyatkin, 2007).

The equation governing heat balance and spatial distribution of brain temperature $T(r)$ has the form (Nelson and Nunneley, 1998; van Leeuwen et al, 2000; Sukstanskii and Yablonskiy, 2006):

$$\rho_{br}c_{br}\frac{\partial T}{\partial t} = \kappa\frac{\partial^2 T}{\partial r^2} - \rho_{bl}c_{bl}\text{CBF}(T - T_{bl}) + G_{ATP}/U_{br}, \quad (9)$$

where κ is the arithmetic mean of the thermal conductance of brain tissue (including cerebrospinal fluid, skull, and scalp at the edge), ρ_{bl} and c_{bl} denote blood's density and specific heat, CBF is the cerebral blood flow rate expressed in sec^{-1} , T_{bl} is the incoming blood (arterial) temperature equivalent to body core temperature, and G_{ATP} is the heat (per time unit) generated in the gray matter due to Na^+/K^+ -ATPase. In general, $G_{ATP} > P_{ATP}$ because P_{ATP} is the useful work (per time unit) performed due to hydrolysis of ATP and release of G_{ATP} of free energy (per time unit). In Sec. 3.5 we estimate the relative magnitude of G_{ATP} and P_{ATP} , i.e., we calculate the efficiency of the sodium pump. The parameter U_{br} denotes brain volume, i.e., $U_{br} = U_g + U_w$ (brain geometry is modelled as half of a ball; Fig. 1). The parameters ρ_{br} and c_{br} denote

brain tissue density and specific heat and they are approximately equal to ρ_{bl} and c_{bl} , respectively. Only steady-state regime of Eq. (9), i.e. $\partial T/\partial t = 0$, is considered below.

The boundary condition imposed on Eq. (9) has the following form:

$$\kappa \frac{\partial T}{\partial r} \Big|_{r=R} = - \left(\sigma_{SB}(T_{sc}^4 - T_o^4) + \eta(T_{sc} - T_o) \right), \quad (10)$$

where R is the brain's radius given by $R = (3U_{br}/2\pi)^{1/3}$, σ_{SB} is the Stefan-Boltzmann constant, η is the heat convection/conduction coefficient between the scalp and the outside environment, and T_{sc} and T_o denote the scalp and environment temperatures. The left hand side of Eq. (10) corresponds to the heat rate removed from the scalp per surface area. The right hand side of Eq. (10) is the sum of scalp radiation (term $\sim T_{sc}^4$) and scalp convection/conduction (term $\sim T_{sc}$). The presence of the term proportional to T_o^4 is a consequence of the fact that scalp not only radiates energy to the environment, but it also receives some radiation from it.

The heat removed from the brain through the conduction is given by

$\dot{Q}_c = -\kappa \int d^3r \partial^2 T / \partial r^2 = -2\pi R^2 \kappa \partial T / \partial r|_{r=R}$. The heat removed by the circulating cerebral blood is given by $\dot{Q}_{bl} = \rho_{bl} c_{bl} \text{CBF} \int d^3r (T(r) - T_{bl})$. Therefore, by integrating Eq. (9) for the whole brain volume, at the steady-state, we obtain:

$$G_{ATP} = \dot{Q}_c + \dot{Q}_{bl}, \quad (11)$$

where the conduction term \dot{Q}_c is a sum of scalp convection/conduction and scalp radiation, i.e., $\dot{Q}_c = \dot{Q}_{cv} + \dot{Q}_r$, with $\dot{Q}_{cv} = 2\pi R^2 \eta (T_{sc} - T_o)$ and $\dot{Q}_r = 2\pi R^2 \sigma_{SB} (T_{sc}^4 - T_o^4)$. Values of all thermodynamic parameters are presented in Table 1.

3 Results

3.1 Sodium influx during a single action potential.

When synaptic fluctuations cause the neuron to fire an action potential, the Na^+ concentration first rise and then slowly decays to its equilibrium value, due to the workings of the Na^+/K^+ pump. Sodium influx during a single action potential can be estimated using Eqs. (2) and (6). It is composed of the two contributions (Fig. 2A): Na^+ influx during a rising phase of sodium conductance g_{Na} and voltage V , and Na^+ influx during a decline phase of g_{Na} and V . The total influx is given by (see Appendix A):

$$\Delta[\text{Na}]_o \approx \frac{4(C + \delta C)}{Fd} (V_{Na} - V_o), \quad (12)$$

where δC denotes ‘‘correction’’ to the effective capacitance coming from the prolonged Na^+ channels activation and is given by $\delta C \approx 0.064 \bar{g}_{Na} \tau_o (V_{Na} - 0.6V_K) / (V_{Na} - V_o)$. Value of τ_o is taken from numerical simulations of Eq. (6), and is approximately $\tau_o \approx 0.4$ msec. This number enables us to determine the parameter δC in Eq. (12), which we find

to be $\delta C \approx 2.4 \mu\text{F}/\text{cm}^2$ for typical resting values of voltages: $V_{Na} = 68 \text{ mV}$, $V_K = -100 \text{ mV}$ (for $[\text{Na}] = 12 \text{ mM}$, $[\text{K}] = 155 \text{ mM}$; Hille, 2001) and $V_o = -67 \text{ mV}$. It should be remembered, however, that δC is not a constant, but it varies slightly depending on the level of intracellular sodium concentration $[\text{Na}]$ via V_{Na} and V_K (see Fig. 2B).

The immediate conclusion from Eq. (12) is that the amplitude of the sodium influx increases with decreasing the effective fiber diameter d , and this agrees with a direct numerical integration of Eq. (6), as is shown in Fig. 2C. Based on the above values, we find from Eq. (12) that for $d = 0.45 \mu\text{m}$ (harmonic mean of average axon and dendrites diameters in mouse; Sec. 2.2) the sodium influx $\Delta[\text{Na}]_o \approx 0.42 \text{ mM}$, which corresponds to $\sim 2.5 \cdot 10^5 \text{ Na}^+$ ions per μm^3 . For a mouse neuron with equal volume of axons and dendrites, and with $l_a = 4 \text{ cm}$ and $d_a = 0.3 \mu\text{m}$, this gives the total influx of $14.2 \cdot 10^8 \text{ Na}^+$ ions. Direct numerical integration of Eq. (6) for $d = 0.45 \mu\text{m}$ yields a similar sodium influx, $\Delta[\text{Na}]_o \approx 0.47 \text{ mM}$, which corresponds to the total influx of $15.9 \cdot 10^8 \text{ Na}^+$ ions for a mouse neuron.

The influx of $14.2 - 15.9 \cdot 10^8 \text{ Na}^+$ ions during an isolated action potential obtained above is comparable to the estimate of Attwell and Laughlin (2001), who used a different, phenomenological, approach and obtained a slightly lower value of $11.5 \cdot 10^8 \text{ Na}^+$ ions. The difference can be attributed to the differences in the assumption regarding spatial properties of the membrane potential and the amplitude of depolarization during an action potential. In this paper, it is assumed that the membrane is equipotential, i.e., axons and dendrites are depolarized by the same amount (135 mV), whereas Attwell and Laughlin (2001) assume that dendrites are 50 % less polarized than ax-

ons (dendrites 50 mV, axons 100 mV). Below, it is shown that the formula for Na^+ charge influx used by these authors is equivalent to the formula (12), if we assume that the axon depolarization ΔV_a during an action potential is the same as the dendrite depolarization ΔV_d . The total charge influx Q_{AL} in Attwell and Laughlin (2001) is $Q_{AL} = 4\pi C(l_a d_a \Delta V_a + l_d d_d \Delta V_d)$, if we neglect a small soma contribution. The prefactor of 4 was chosen by these authors to a large extent arbitrary, and it comes from the effect of simultaneous activation of Na^+ and K^+ channels, which is analogous to the presence of the δC contribution in Eq. (12). Now, assuming that $\Delta V_d = \Delta V_a \equiv \Delta V$, and noting that $Q_{AL} = F U_n \Delta[\text{Na}]_{AL}$, where $\Delta[\text{Na}]_{AL}$ is the sodium influx in the Attwell and Laughlin (2001) formulation, we obtain $\Delta[\text{Na}]_{AL} = 16C\Delta V/(Fd)$, where d is the effective fiber diameter defined in Eq. (3). The formula for $\Delta[\text{Na}]_{AL}$ is very similar to the formula (12), except for the numerical factor in front, which is 13.6 in Eq. (12). This results from the fact that numerically $\delta C = 2.4C$ for low firing rates or intracellular sodium concentrations (Fig. 2B). It is also interesting to note that the Attwell-Laughlin (2001) formula does not account for changes in the intracellular Na^+ concentration due to repetitive firing, as opposed to Eq. (12) that includes such changes through δC . In this sense Eq. (12) extends the phenomenological approach of these authors into the broader range of frequencies.

3.2 Sodium build-up due to repetitive firing.

When the neuron fires repeatedly, its intracellular sodium accumulates with every spike because Na^+/K^+ pump is slow and cannot remove all Na^+ promptly (Fig. 3A,B). Since every spike introduces $U_n F \Delta[\text{Na}]_o$ of sodium electric charge, and this process is fast,

we can approximate Eq. (6) for the Na^+ dynamics as

$$U_n F \frac{d[\text{Na}]}{dt} \approx I_o + U_n F \Delta[\text{Na}]_o \sum_i \delta(t - t_i) - \frac{3AS[\text{Na}]^k}{[\text{Na}]^k + \theta^k}, \quad (13)$$

where I_o is the sodium current associated with sodium channels and synaptic contribution at rest, and it is given by $I_o = \{g_{\text{Na},o} + q(f)f\rho_s dg_s \tau_s V_K / (4(1 - \phi)(V_K - V_{\text{Na}}))\} S(V_{\text{Na}} - V_o)$. The delta functions present in Eq. (13) represent spikes of Na^+ influx at times t_i . Simulation of Eq. (13) is shown in Fig. 3C, and it resembles the simulation of the original Eq. (6) (see Fig. 3A).

We can further simplify Eq. (13) at the long-time limit, in which we substitute for the right hand side of Eq. (13) its temporal average. In particular, the temporal average of $\sum_i \delta(t - t_i)$ is equal to the firing rate f , and thus

$$U_n F \frac{d\overline{[\text{Na}]}}{dt} \approx I_o + f U_n F \Delta[\text{Na}]_o - \frac{3AS\overline{[\text{Na}]^k}}{\overline{[\text{Na}]^k} + \theta^k}, \quad (14)$$

where $\overline{[\text{Na}]}$ is the temporal average of $[\text{Na}]$. A comparison of the time dependence of $\overline{[\text{Na}]}$ from Eq. (14) with the time dependence of $[\text{Na}]$ coming from Eq. (13) is presented in Fig. 3C. The equilibrium value of $\overline{[\text{Na}]}$, denoted as $[\text{Na}]_{av}$ is determined from the condition $d\overline{[\text{Na}]} / dt = 0$, with the help of Eq. (12). $[\text{Na}]_{av}$ satisfies the following equation:

$$\frac{3A[\text{Na}]_{av}^k}{[\text{Na}]_{av}^k + \theta^k} \approx I_o / S + f(C + \delta C)(V_{\text{Na}} - V_o). \quad (15)$$

Note that the right hand side of Eq. (15) also depends on $[\text{Na}]_{av}$ through V_{Na} and δC . Thus, we can find $[\text{Na}]_{av}$ only numerically, either from Eq. (15) or from a direct simulation of Eq. (14).

In Fig. 4, we compare the dependence of $[\text{Na}]_{av}$ on firing rate that comes from Eq. (15) with the dependence that comes from a direct numerical integration of Eq. (6). Overall, the formula (15) provides a relatively good approximation to the numerical solution, especially for low firing rates (Fig. 4). For this reason, it is used in the following sections to approximate metabolic expenditure and thermal changes in the brain tissue.

It is interesting to note that the average $[\text{Na}]_{av}$ is weakly dependent on fiber diameter, especially for small firing rates (Fig. 4). The reason for this is that only the current I_o in Eq. (15) contains synaptic contribution with d , and for low frequencies I_o is small.

It should be kept in mind, however, that sodium fluctuations around $[\text{Na}]_{av}$ do grow with decrease in fiber diameter (Fig. 3B), because for thin fibers the amplitude of sodium influx is large ($\Delta[\text{Na}]_o \sim 1/d$) and the relaxation time constant is short ($\tau \sim d$; see Appendix B). Enhanced intracellular sodium fluctuations can effectively reduce the concentration gradients across neuron's membrane to values close to zero, and this would have a devastating effect on neuron's functionality if high firing rates were maintained for a prolonged period of time. For example, for $d = 0.11 \mu\text{m}$ corresponding to the smallest physically possible axons of $d_a = 0.06 \mu\text{m}$ (Faisal et al, 2005) the intracellular sodium concentration can occasionally peak to extracellular levels (145 mM; Hille 2001)

just for 40 Hz of repetitive firing. For $d = 0.45 \mu\text{m}$ (corresponding to $d_a = 0.3 \mu\text{m}$) this takes place for ~ 50 Hz. These considerations suggest that very thin fibers are not beneficial for neuron's electrical properties.

3.3 ATP utilization rate of Na^+/K^+ pump, glucose metabolism, and firing rate in mammals.

For pumping out Na^+ and pumping in K^+ , the Na^+/K^+ pump uses ATP molecules. The average ATP utilization rate of a single neuron per its surface area S is equal to $I_{p,av}/(FS)$. Generally, it increases with $[\text{Na}]_{av}$ and thus with the firing rate f in a non-linear fashion (Fig. 5A). For low frequencies f there exist a linear regime, while for high f , the ATP rate saturates reaching its maximum value A/F (Fig. 5A). Typical values of ATP utilization for frequencies in the range 1 – 10 Hz are $(0.6 - 9) \cdot 10^4$ ATP molecules per μm^2 per second. In the linear regime, the increase of firing rate by 1 Hz leads to the increase of the ATP rate by about $1.7 \cdot 10^{-4} \mu\text{mol}/(\text{cm}^2\text{sec})$. It is important to point out that in previous phenomenological models of ATP utilization rate (Attwell and Laughlin 2001; Lennie, 2003) only linear regime was assumed in estimations. Thus, the present more detailed model extends these calculations into the non-linear regime.

The average firing rate in mammalian brains can be determined indirectly from the cerebral glucose utilization rates CMR_{glu} (expressed in $\text{mol}/(\text{cm}^3 \cdot \text{s})$). If we assume that the ATP activity of the neural pumps constitutes the major contribution to the gray matter metabolism (Astrup et al, 1981; Erecinska and Silver, 1989; Rolfe and Brown, 1997; Ames 2000), then we can relate directly the ATP rate or the pump current to CMR_{glu} . Since 31 ATP molecules are produced per 1 glucose molecule

(Rolfe and Brown, 1997), we have for the whole gray matter the following equality $31U_g\text{CMR}_{glu} = NI_{p,av}/F$, from which we obtain, using Eq. (4), that

$$\text{CMR}_{glu} = \frac{4(1 - \phi)A[\text{Na}]_{av}^k}{31Fd([\text{Na}]_{av}^k + \theta^k)}. \quad (16)$$

We can write CMR_{glu} in an equivalent form, which contains neurophysiological parameters explicitly. Using Eq. (15), we obtain:

$$\text{CMR}_{glu} \approx \frac{4(1 - \phi)}{93Fd} (I_o/S + f(C + \delta C)(V_{Na} - V_o)). \quad (17)$$

Dependence of CMR_{glu} on firing rate f is plotted in Fig. 5B, and it is practically the same as the dependence of $I_{p,av}$ on f , as the two quantities CMR_{glu} and $I_{p,av}$ are proportional. The non-linear part of the dependence comes from the fact that δC and V_{Na} decrease for high frequency (via $[\text{Na}]_{av}$). The CMR_{glu} vs. f relationship (Eq. 17) enables us to find average frequencies for several mammalian species for which empirical values of CMR_{glu} are known (Fig. 5C). In general, the average firing rates are rather low, from ~ 1.7 Hz for human to ~ 6.2 Hz for mouse (Table 2). Moreover, estimated in such a way average firing rates scale with gray matter volume with an exponent of -0.15 (Fig. 5C), implying that average activity in larger brains is slower than in smaller brains.

3.4 Biphasic dependence of pump power on frequency.

The electric power generated by the Na^+/K^+ pump in a single neuron (per surface area) is determined in two ways. First, from a direct numerical integration of Eq. (7) with time dependent voltage V and pump current I_p . Second, from the approximate analytical formula (8) with the help of derived Eq. (15). Both methods yield similar results (Fig. 6A), which indicates that the approximation (8) is reliable, especially for low firing rates. We can rewrite Eq. (8) for the total electric power generated in the gray matter in a more convenient form using Eq. (4). The result is

$$P_{ATP} \approx \frac{4(1-\phi)U_g A [\text{Na}]_{av}^k}{d([\text{Na}]_{av}^k + \theta^k)} (3V_{Na} - 2V_K - V_o). \quad (18)$$

Alternatively, we can use Eq. (15) to relate the pump current to the neurophysiological parameters. In this way, we obtain:

$$P_{ATP} \approx \frac{4(1-\phi)U_g}{3d} (3V_{Na} - 2V_K - V_o) (V_{Na} - V_o) \times \left(g_{Na,o} + \frac{fq\rho_s dg_s \tau_s V_K}{4(1-\phi)(V_K - V_{Na})} + f(C + \delta C) \right). \quad (19)$$

Note that synaptic depression via q reduces the power P_{ATP} . In Eq. (19) the first term in the large bracket represents a very small sodium influx at rest, the second term corresponds to the background dendritic synaptic activity, and the last term comes from Na^+ influx due to action potentials. The relative contribution of these 3 elements

to P_{ATP} depends on firing rate f . For example, for $f = 1.7$ Hz, corresponding to the estimate for human brain (Table 2), sodium influx at rest constitutes 5 %, background dendritic synaptic activity 15 %, and Na^+ influx due to action potentials yields 80 % of the total power.

Fig. 6A indicates that P_{ATP} depends biphasically on firing rate f . This is a non-intuitive result, following from the fact that P_{ATP} is a product of two terms: I_p and $(3V_{Na} - 2V_K - V_o)$. The first of them increases monotonically with f , whereas the second decreases with f because V_{Na} and V_K depend on frequency via $[\text{Na}]_{av}$. This biphasic dependence of P_{ATP} on frequency has interesting implications for thermal properties of brain tissue, which are discussed in the subsection (3.7). From the estimated firing rates for several mammalian species we can also estimate, based on Eq. (19), their P_{ATP} rates (Table 2).

The sodium pump power P_{ATP} also depends inversely on the fiber diameter d (Eq. (19) and Fig. 6B), and proportionally on the gray matter volume U_g . Thus, too thin fibers are metabolically expensive.

The power generated by the sodium pumps in the gray matter can be related directly to the glucose cerebral metabolic rate CMR_{glu} if we combine Eqs. (16) and (18). The resulting relationship is:

$$P_{ATP} \approx 31FU_g(3V_{Na} - 2V_K - V_o)\text{CMR}_{glu}. \quad (20)$$

Thus, the power generated scales linearly with the glucose consumption rate. However,

it should be kept in mind that the proportionality factor is not a constant, but changes with firing rate.

3.5 Efficiency of the Na^+/K^+ pump.

Let us estimate the efficiency of the sodium pump, i.e., how much energy does it use for pumping out 3 Na^+ and pumping in 2 K^+ ions given an available energy from ATP hydrolysis. Energy from hydrolysis of 1 ATP molecule goes for performing the useful work of $-3e(V - V_{Na}) + 2e(V - V_K)$, or equivalently 1 mole of ATP performs the work of $F(3V_{Na} - 2V_K - V_o)$, where e is the electron charge. On the other hand, hydrolysis of 1 mole of ATP generates J_{ATP} of free energy. Thus, the efficiency of the process is given by $F(3V_{Na} - 2V_K - V_o)/J_{ATP}$. The value of J_{ATP} depends to some extent on the internal chemical (ionic) state of the cell, and it has been reported to be in the range from 48 kJ/mol (Jansen et al, 2003) to 62 kJ/mol (Erecinska and Silver, 1989). This leads to the pump efficiency of 73 – 95 % (for typical resting values of voltages: $V_{Na} = 0.068$ V, $V_K = -0.100$ V, $V_o = -0.067$ V; Hille (2001)). Because of the high efficiency of the Na^+/K^+ -ATPase, in what follows, we make an approximation in which we equate the heat released in the gray matter due to hydrolysis of ATP (G_{ATP} in Eq. 9) with the electrical power dissipated by the pump (P_{ATP} in Eq. 7).

We can estimate the heat rate for the gray matter of human brain from Eq. (20). Taking $U_g = 680$ cm^3 (Stephan et al, 1981), $CMR_{glu} = 5.7 \cdot 10^{-9}$ $\text{mol}/(\text{cm}^3 \cdot \text{sec})$ (or 0.34 $\mu\text{mol}/(\text{cm}^3 \cdot \text{min})$; e.g. Clarke and Sokoloff, 1994), and for the above values of voltages we obtain $P_{ATP} \approx 5.5$ Watts. Given a possible increase of this heat value by up to 27% due to pump efficiency, this result does not differ much from other estimates of

heat in gray matter. For example, Aiello and Wheeler (1995) used mass specific heat generation of 11.2 W/kg (based on older experimental data), which yields 7.8 Watts for the human gray matter.

3.6 Scaling of cerebral blood flow with brain size.

Cerebral blood flow CBF is important in controlling brain temperature (see the next subsection). The dependence of physiologically averaged CBF on brain volume can be found from the empirical data available in the literature. The results in Fig. 7 for 6 mammals spanning 3 orders of magnitude in brain size show that CBF scales systematically with brain volume as $CBF = 0.018U_{br}^{-0.10}$ 1/sec. This implies that cerebral blood flow decreases weakly as brains increases in size, ranging from $\sim 0.020 \text{ sec}^{-1}$ for mouse to $\sim 0.009 \text{ sec}^{-1}$ for human.

3.7 Brain temperature vs. frequency and fiber diameter, and efficiency of brain cooling

The spatial distribution of brain temperature $T(r)$ is found by solving Eq. (9) with $G_{ATP} = P_{ATP}$, and the result is given by (see Appendix C):

$$T(r) = T_{bl} + \frac{P_{ATP}}{\rho_{bl}c_{bl}U_{br}CBF} - \frac{(\sigma_{SB}(T_{sc}^4 - T_o^4) + \eta(T_{sc} - T_o))}{(\kappa\rho_{bl}c_{bl}CBF)^{1/2}} e^{-\xi(R-r)}, \quad (21)$$

where $\xi = (\rho_{bl}c_{bl}CBF/\kappa)^{1/2}$. The parameter ξ characterizes the inverse of the length of “transition” region from the scalp to the brain’s interior where temperature is inhomogeneous (Fig. 8A). For human $\xi^{-1} \approx 0.4 \text{ cm}$, and it is much smaller than human

brain radius (≈ 8 cm), and thus heterogeneity is present only at the brain’s edge. On the contrary, for mouse $\xi^{-1} \approx 0.25$ cm, i.e., it is comparable with the mouse brain radius (≈ 0.4 cm), implying that in very small brains cerebral temperature is inhomogeneous in the whole volume (Fig. 8A). The scalp temperature T_{sc} present in Eq. (21) is determined self-consistently (see Appendix C) from the condition $T_{sc} = T(R)$, and it decreases very weakly with brain volume (Table 2). Its value for human, $T_{sc} = 34.7^\circ\text{C}$, is similar to experimental values ($34 - 35^\circ\text{C}$; Hensel et al, (1973)).

Deep brain temperature $T(0)$ is slightly larger than the blood temperature by $0.1 - 0.2$ °C for all analyzed mammals, except mouse (Table 2). This value lies in the range of values observed experimentally (Hayward and Baker, 1968; Nybo et al, 2002; Kiyatkin, 2007). In general, however, $T(0)$ is very weakly species specific. For large enough brains $T(0)$ is approximately $T(0) \approx T_{bl} + P_{ATP}/(\rho_{bl}c_{bl}U_{br}\text{CBF})$, which shows that the boundary temperature (and scalp cooling) becomes unimportant in this limit. From this formula it follows that the deep brain temperature is greater than the blood (or core body) temperature by the quantity proportional to the ratio of CMR_{glu} to CBF, in agreement with Yablonskiy et al (2000). This result suggests for example that, for a given animal, any local increase in the cerebral blood flow that exceeds an increase in glucose utilization rate leads to a lowering of brain temperature, and vice versa.

Deep brain temperature $T(0)$ depends significantly on the effective fiber diameter d (Fig. 8B,C). For very small d (corresponding to very small d_a), the temperature $T(0)$ tends to diverge, which is a direct consequence of the fact that P_{ATP} also diverges for $d \rightarrow 0$ (or equivalently $d_a \rightarrow 0$). In this “thin fiber” limit we have a simple inverse

proportionality (see Eqs. (19) and (21)) between brain-body temperature difference and fiber thickness, i.e., $T(0) - T_{bl} \sim 1/d \sim 1/(2d_a)$. This relationship implies that decreasing fiber diameter twofold increases $T(0) - T_{bl}$ by the same amount. This suggests again that too thin fibers are not beneficial for brain thermal equilibrium and hence its functioning.

In contrast to the monotonic dependency of $T(0)$ on d , its dependence on firing rate is biphasic (Fig. 8D). The origin of this non-monotonic behavior is the dependence of P_{ATP} on f , which is also biphasic (see Fig. 6A). This result has surprising thermodynamic consequences, namely too high levels of neural activity (firing rate) can lead to a decrease in the cerebral tissue temperature. For human brain, corresponding changes in temperature are rather small, at the peak about 0.5-0.6 K (Fig. 8D), which falls into the range of values reported experimentally (Yablonskiy et al, 2000; Kiyatkin, 2007).

In the superficial regions brain temperature is always smaller than the blood temperature (Fig. 8A; Table 2). This fact has important consequences for the heat transfer in the mammalian brains. In deep brain regions cerebral blood flow plays the role of a coolant, whereas in the superficial regions it serves as a strong brain heater. Consequently, the net effect of blood flow is to warm up the brain tissue, i.e., $\dot{Q}_{bl} < 0$ (Table 2).

In general, the cooling mechanisms discussed in subsection (2.5) depend on brain temperature distribution, on scalp temperature T_{sc} , and on brain volume U_{br} . Therefore, the efficiency of cerebral cooling is species specific. In particular, the relative importance of the two major mechanisms of heat transfer inside the brain is dependent on brain

size. For very small brains, heat cooling rate via conduction \dot{Q}_c is comparable to the heat warming rate via blood flow \dot{Q}_{bl} (Table 2). The reason for such a strong warming through the cerebral blood is that it must compensate heat loss due to scalp convection/conduction \dot{Q}_{cv} and radiation \dot{Q}_r , which are much larger than the metabolic rate P_{ATP} . On the other hand, for large brains, the cooling rate \dot{Q}_c is almost twice as large as the warming rate \dot{Q}_{bl} , because heat production due to metabolic activity P_{ATP} is more significant than for small brains (Table 2). On the scalp, the heat transfer rate is dominated by convection/conduction \dot{Q}_{cv} , as it is twice the radiation rate \dot{Q}_r .

3.8 Thermal bounds on fiber diameter and length.

Mammals are able to sustain brain temperatures up to about 42 °C without causing brain damage (Gordon, 1993; Kiyatkin, 2007). Above these temperatures molecular changes in neurons and synapses become critical and irreversible. In what follows, we estimate the thermal bounds on fiber diameter that allow to maintain the safe temperature regime. For this purpose we use Eq. (21) for $r \approx 0$, in which we put $\Delta T_{max} \equiv T(0) - T_{bl} = 5$ K, as the largest possible difference between brain and blood temperatures. Solving Eq. (21) for the effective fiber diameter d , we obtain

$$d \geq d_{min} = \frac{4(1 - \phi)U_g (g_{Na,o} + f(C + \delta C))}{\frac{3\rho_{bl}c_{bl}U_{br}CBF\Delta T_{max}}{(V_{Na}-V_o)(3V_{Na}-2V_K-V_o)} - \frac{fq\rho_s g_s \tau_s V_K U_g}{(V_K - V_{Na})}}, \quad (22)$$

where we used Eq. (19) for P_{ATP} . The minimal effective fiber diameter d_{min} depends very weakly on gray matter volume U_g (Fig. 9A). This suggests that brain size is not a

critical factor determining thermodynamic safety of the cerebral tissue. In other words, thermal properties of mouse and elephant brains, differing by 4 orders of magnitude in size, are rather similar.

The minimal effective fiber diameter d_{min} depends stronger and biphasically on firing rate f (via V_{Na} , V_K , and $[Na]_{av}$) (Fig. 9B). For very low firing rates ($f \rightarrow 0$), the expression (22) simplifies, and we obtain in this limit:

$$d_{min} \approx \frac{4(1 - \phi)g_{Na,o}(V_{Na} - V_o)(3V_{Na} - 2V_K - V_o)U_g}{3\rho_{bl}c_{bl}U_{br}CBF\Delta T_{max}}, \quad (23)$$

which yields ≈ 0.3 nm (values of U_g and U_{br} are for human brain). For intermediate values of f , for which d_{min} has a maximum, the value of d_{min} can be in the range $0.04 - 0.05$ μm (Fig. 9B), which corresponds to a bound on axon diameter $d_a = 0.02 - 0.03$ μm . The latter value is only about 5 times larger than the membrane thickness (Koch, 1998). The term proportional to fq in the denominator of Eq. (22) is the background synaptic contribution with frequency dependent depression inside q . Due to this depression the synaptic contribution is bounded from above and consequently does not diverge as a function of f . Thus, synaptic depression not only reduces the power P_{ATP} (see. Eq. 19), but it also makes d_{min} finite. Without depression, the bound d_{min} would diverge for $f \sim 450$ Hz.

Average value of the empirical fiber diameter d in the gray matter is brain size independent and is about 0.45 μm (harmonic mean of average axon and dendrite diameters in mouse, as defined in Sec. 2.2, Eq. (3)). This value is about 10 times larger than

the largest value of d_{min} . Because of this, mammalian brains operating under normal physiological conditions are rather safe from excessive overheating that would cause brain damage, for all ranges of frequency. The situation could be more tricky in hot environments in which ΔT_{max} were severely reduced, due to increase in body temperature and hence cerebral blood temperature. The margins of thermal safety, could be also compromised in pathological conditions. For example, abnormalities associated with strongly reduced cerebral blood flow CBF or compromised synaptic depression, could significantly increase the bound d_{min} up to the lower neuroanatomical values of d .

The thermal lower bound on fiber diameter also determines the upper bound on fiber length per neuron l , as is evident from Eq. (4). Taking the neuron's surface area $S = \pi ld$, we get $l \leq 4(1 - \phi)U_g/(\pi N d_{min}^2)$, where $d_{min} = 0.01 - 0.05 \mu\text{m}$. For human brain with $U_g = 680 \text{ cm}^3$ (Stephan et al, 1981) and $N = 2 \cdot 10^{10}$ (Haug, 1987; Braendgaard et al, 1990) this yields $l \leq 12 - 300$ meters. For mouse brain with $U_g = 0.11 \text{ cm}^3$ and $N = 1.6 \cdot 10^7$ (Braitenberg and Schuz, 1998) we get $l \leq 2.4 - 60$ meters. Neuroanatomical data for mouse gray matter indicate that the average fiber length per neuron is $1.5 - 4.5 \text{ cm}$ (Braitenberg and Schuz, 1998), which is 2-3 orders of magnitude below its upper thermal bound. A similar conclusion holds for the human brain.

Taken together all these results suggest that thermodynamics does not restrict neuroanatomical parameters in any dramatic way, because they are far away from their thermal bounds.

4 Discussion

This article investigates thermodynamic properties of brain tissue and corresponding physical limits on neural anatomy caused by heat balance in the brain. It is found that, in general, the lower and upper limits on fiber dimensions are unattainable for normal values of physiological parameters such as cerebral blood flow and maximal Na^+/K^+ -ATPase. This suggests that real mammalian brains either keep these physiological parameters in the “proper” range or scale appropriately average fiber diameter and length to maintain wide margins of thermodynamic safety. Such wide margins presumably enable the brain to avoid overheating during enhanced cerebral activities, abnormal states (e.g. epileptic seizures), and in hot environments.

The conclusions of this paper are based on calculating neural metabolic power and spatial distribution of heat dissipated. Since majority of metabolic energy in neurons goes to pumping out sodium ions (Ames, 2000; Astrup et al, 1981; Erecinska and Silver, 1989; Rolfe and Brown, 1997), the first step in determining neural power was to find Na^+ influx during an action potential. An explicit analytical formula for this Na^+ influx was derived (Eq. 12) and was validated numerically. This analytical formula yields similar results for an isolated action potential as the one of phenomenological character by Attwell and Laughlin (2001) (20 – 28% discrepancy between the two can be attributed to the different assumptions regarding the magnitude of depolarizations in axons and dendrites). However, for repetitive firing the derived here Eq. (12) extends the Attwell and Laughlin (2001) formula, because it accounts for intracellular sodium accumulation and corresponding changes in membrane electrical properties expressed

by δC (correction to Na^+ influx due to prolonged Na^+ channels activation). Moreover, the sodium build-up is also important for the accurate determination of ATP/glucose utilization rates for high frequencies. In this respect, Eqs. (16) and (17) extend the Attwell and Laughlin (2001), and Lennie (2003) linear calculations to the non-linear regime. An additional novelty in the present approach is inclusion of synaptic depression in the transmission probability.

The issue of brain cooling is not a classic problem of volume to surface ratio, as it is the case with natural, non-designed, physical objects. Instead, the brain cooling could be compared to the cooling of combustion heat engine, which receives a liquid coolant. In the brain the role of the coolant is played by the cerebral blood, but only in the deep region because there blood has a slightly lower temperature than the brain tissue. In the superficial regions brain tissue has a smaller temperature than the cerebral blood, and there blood warms up the brain. The fact that the deep brain temperature depends weakly on brain volume (Table 2), implies that brain size is not a major determinant of thermal responses. This in turn implies that the thermodynamics of heat balance does not restrict the brain size in any significant way, suggesting that, in principle, brains could be heavier than 5 kg (the largest known brain).

The interesting result is that the power generated by the sodium pump depends biphasically on neural frequency of firing, and inversely on the effective fiber diameter (Fig. 6). As a consequence of this, brain temperature $T(0)$ can depend biphasically on frequency as well, if cerebral blood flow does not change with frequency (Fig. 8D). Thus $T(0)$ increases with frequency but only up to a certain point above which it

slightly decreases with further increase in frequency. The increase of brain temperature in response to activation (higher firing rate) is an expected behavior (Kiyatkin, 2007). However, the decrease of $T(0)$ for very large stimulation (very high firing rates) is an unexpected effect that can explain some experimental results in which stimulation of certain brain regions led to lowering of local temperature (McElligott and Melzack, 1967; Yablonskiy et al, 2000). The standard explanation for the decrease of $T(0)$ upon stimulation requires that cerebral blood flow must increase more than P_{ATP} increases (Yablonskiy et al, 2000). The biphasic relationship between temperature and frequency, obtained in this paper (Fig. 8D), offers an alternative explanation, namely, that brain temperature can decrease upon vigorous (or prolonged) stimulation even when cerebral blood flow does not change.

The negative correlation between the power generated in the brain and the effective wire diameter (Fig. 6B) suggests that thin fibers are energy expensive. The effective fiber diameter d is defined as a harmonic mean of axon d_a and dendrite d_d diameters (Sec. 2.2), with the assumption that volumes of axons and dendrites are equal (Braitenberg and Scüz, 1998; Chklovskii et al, 2002). In general, d and d_a are positively correlated and $d \rightarrow 0$ if $d_a \rightarrow 0$. Thin fibers also promote large fluctuations of intracellular sodium concentration in response to stochastic action potentials (Fig. 3B), which can be disadvantageous for electrical properties of neurons.

Another negative consequence of having too thin fibers is that cerebral tissue temperature increases inversely with fiber diameter (Fig. 8C), i.e., $T(0) - T_{bl} \sim 1/d$. Thus, brain regions reach in very thin wire can heat up excessively. As an example, the tem-

perature of the thinnest known axons with diameter $0.1 \mu\text{m}$ (Faisal et al, 2005, i.e. $d = 0.18 \mu\text{m}$), relative to blood temperature, should be about 2.5 times larger than the corresponding relative temperature of $0.3 \mu\text{m}$ axons (mouse cerebral cortex; Braitenberg and Schuz, 1998; corresponding to $d = 0.45 \mu\text{m}$), assuming both axons have the same firing rate. Thus, if typical relative temperatures above blood temperature are $0.2 - 0.3 \text{ }^\circ\text{C}$ for $0.3 \mu\text{m}$ axons (Hayward and Baker, 1968), then for $0.1 \mu\text{m}$ axons the corresponding relative temperatures would be $0.5 - 0.8 \text{ }^\circ\text{C}$. This result suggests an explanation why in the peripheral nervous system sensory fibers responsible for high-threshold heat sensation (so-called C-fibers) are much thinner ($0.1 - 1.5 \mu\text{m}$; Kandel et al, 1991) than other sensory fibers (A-type or B-type with diameters $1 - 5 \mu\text{m}$). It might be that they warm up easier, although these fibers also serve other functions (Craig, 2003).

This study finds that the lower thermal bound on the effective fiber diameter d_{min} is strongly frequency dependent, but it is finite due to synaptic depression. Values of d_{min} are in the range $0.3 - 50 \text{ nm}$ (or $0.0003 - 0.05 \mu\text{m}$; see Fig. 9B). These values can be translated to the corresponding thermal bounds on axon diameter d_a , which are in the range $0.0002 - 0.026 \mu\text{m}$ (assuming that the dendrite diameter $d_d = 0.9 \mu\text{m}$ and it does not change). The average value of cortical axon diameter is $d_a = 0.3 \mu\text{m}$, and thus it is 12-1500 times larger than these limits, therefore, on average, mammalian brains operate in the safe thermal zone. However, it should be also kept in mind that axon diameter displays some variability, and the thinnest axons can reach $0.1 \mu\text{m}$ (Faisal et al, 2005). This value is still about 4 times larger than the maximal value of the

lower thermal limit on d_a (which is $0.026 \mu\text{m}$), suggesting that thermal limits are not an immediate constraint on fiber size. It is also interesting to note that the estimated maximal lower thermal bound on the diameter of brain axonal wiring ($0.026 \mu\text{m}$) is smaller than corresponding bounds imposed by structural constraints and noise, which are respectively $0.06 \mu\text{m}$ and $0.1 \mu\text{m}$ (Faisal et al, 2005).

The theoretical bound on axon diameter implies a corresponding lower bound on the speed of signal propagation in the gray matter. Let us estimate the upper limit on temporal delays. For unmyelinated fibers (prevalent in gray matter) velocity of signal propagation is proportional to the square root of the fiber diameter (Hodgkin, 1954). Experimentally, for axons with $d = 1 \mu\text{m}$ the propagation velocity is 2.3 mm/msec (Koch, 1998), which implies that for axons with the boundary thickness of $0.026 \mu\text{m}$, we have velocities 0.37 mm/msec . This gives for the maximal known extent of axons in the gray matter of 9-10 mm (for macaque monkey visual cortex; Amir et al, (1993)) the upper limit on delays in the range 24-27 msec. Thus, apparently, thermodynamics of heat balance in the gray matter does not tolerate temporal axonal delays longer than $\sim 0.03 \text{ sec}$, which is a stringent constraint.

The problem of finding bounds on fiber dimensions is similar in spirit to the approaches of “wire minimization” in the brain (Cherniak 1995; Murre and Sturdy 1995; Karbowski 2001, 2003; Chklovskii et al, 2002). It is hypothesized that this principle governs the organization of the mammalian nervous system at different scales (Murre and Sturdy 1995; Prothero, 1997; Kaas 2000; Karbowski 2001, 2003), because it offers energy savings associated with ionic membrane transport, as well as reduction in

temporal delays in neural communication. The heat balance limits on fiber diameter, found in this paper, suggest corresponding upper thermal bounds on the density of wire packing in the brain in the range 20 – 100 fibers per μm . These thermal bounds on wire density are a factor of 2-4 higher than the corresponding upper bounds coming from structural and noise considerations (Faisal, 2005).

The estimated firing rates in mammals are in the range from 1.7 Hz for human to 6.2 Hz for mouse, and they scale systematically with brain size, with the exponent -0.15 (Fig. 5C). The estimate for rat (5 Hz) is very close to that assumed by Attwell and Laughlin (2001), i.e. 4 Hz, which was based on weighted average of values observed experimentally. Also the estimate for cat (4.5 Hz) is reasonably close to that reported experimentally for visual cortex (2.5-4.0 Hz; see Baddeley et al, 1997). However, *in vivo* values of firing rates are stimulus dependent and in many species are largely unknown. The scaling result of firing rates is qualitatively consistent with the experimental data on avian brains, which show an allometric decay of firing rates in the peripheral nervous system with brain/body mass (Hempleman et al, 2005). It is also consistent with a prediction coming from a recent analysis of empirical data on brain metabolic scaling in mammals (Karbowski, 2007), where it was suggested that an average firing rate should decrease for bigger brains to account for a negative allometric exponent of specific metabolic rate, which was also -0.15 . This conclusion is analogous to the general trend in mammals, in which physiological processes tend to slow down with an increase in body size (Schmidt-Nielsen 1984).

The estimate of the heat generated in the gray matter may have some margins of

error. First, the assumption of the equipotential neuron is only an approximation, because it does not include explicitly the spatio-temporal effects associated with action potential propagation and back-propagation. However, it is estimated in Appendix A that the correction from this effect is rather small of the order of 16%, i.e., the actual Na^+ influx can be larger by this amount. Second, because the efficiency of the pump is a little less than 100% (73 – 95 %; Sec. 3.5), the actual heat dissipated in the gray matter may be larger than P_{ATP} by 5 – 27 %. Therefore the total error from these two effects on the cerebral heat can theoretically reach 43%. We should also remember that some heat coming from the glucose to ATP conversion was neglected (i.e., it is assumed that glycolysis is 100% efficient). However, the comparison of the heat estimates for the human gray matter indicates that in fact the total heat error cannot be larger than 30% (Sec. 3.5). There are also other sources of error that affect the temperature distribution in the brain, such as the neglect of cooling by scalp perspiration, and variability of environmental T_o temperature, which can affect convection/conduction and radiation cooling rates. However, these contributions should not have any dramatic influence on the thermal properties of brain tissue. Moreover, neither of these sources of error or their combination seem to affect the main conclusion of this paper, namely, that neural anatomy (fiber diameter and its length) does not approach its thermodynamic limits. To reach these limits the ratio of the maximal sodium pump current to the cerebral blood flow would have to be at least 10-100 times larger.

The formulas (Eqs. 17-21) in this paper for the CMR_{glu} , power dissipated in the gray matter, and brain temperature, may have practical use. These formulas as well as

their possible future extensions can be used for assessing neural activity (firing rates) based on changes in temperature, CMR_{glu} , and CBF. Moreover, because this study offers a direct relationship between neural activity and neuroanatomical parameters, it may be useful in quantitative studies of the interplay between brain development, evolution, and metabolism (Purves, 1988; Striedter, 2005).

Acknowledgments

The work was partly supported by the Caltech Center for Biological Circuit Design. I acknowledge useful suggestions of the two anonymous reviewers.

Appendix A: Sodium influx during an action potential.

The duration of a typical action potential can be divided into two phases (Fig. 2A). During the first phase Na^+ conductance g_{Na} rises almost instantaneously to its maximal value \bar{g}_{Na} and voltage V increases to its peak value V_{Na} . The second phase is characterized by decline in values of g_{Na} (to zero) and V (to values < 0). The total Na^+ influx during an action potential is $\Delta[Na]_o = \Delta[Na]_o^{(1)} + \Delta[Na]_o^{(2)}$, where superscripts (1) and (2) refer to the first and second phase, respectively.

During the first phase, the intracellular potassium concentration practically does not change, because K^+ channels are activated with a delay. Thus, by straightforward integration of Eq. (2), we obtain the Na^+ influx during this phase as:

$$\Delta[\text{Na}]_o^{(1)} \approx \frac{4C}{Fd}(V_{Na} - V_o), \quad (24)$$

where the contribution proportional to g_L was neglected, since it is much smaller.

Sodium influx during the second phase can be computed from the sodium dynamics of Eq. (6). Most of the time during this phase, the term proportional to g_{Na} is much larger than the remaining two terms in Eq. (6). Thus, we can write

$$\Delta[\text{Na}]_o^{(2)} \approx -\frac{4}{Fd} \int_0^{\tau_o} dt g_{Na}(t)(V(t) - V_{Na}), \quad (25)$$

where τ_o is the duration of the second phase and $\tau_o \approx 0.4$ msec (from simulations). To simplify calculations, it is assumed that Na^+ conductance and voltage depend on time in the following way: $g_{Na}(t) \approx \bar{g}_{Na}(1 - t/\tau_o)$ and $V(t) \approx V_{Na} + (0.6V_K - V_{Na})(t/\tau_o)^z$. These forms assure that for $t = 0$, we have $g_{Na}(0) \approx \bar{g}_{Na}$ and $V(0) \approx V_{Na}$, and for $t = \tau_o$ we have $g_{Na}(\tau_o) \approx 0$ and $V(\tau_o) \approx 0.6V_K$. The latter value comes from simulations. After performing integral in Eq. (25) we obtain:

$$\Delta[\text{Na}]_o^{(2)} \approx \frac{4\bar{g}_{Na}\tau_o(V_{Na} - 0.6V_K)}{Fd(z+1)(z+2)} \quad (26)$$

The fits in Fig. 4 are made for $z = 2.5$. The total Na^+ influx during an action potential is $\Delta[\text{Na}]_o^{(1)} + \Delta[\text{Na}]_o^{(2)}$, and is given by Eq. (12) in the main text.

It is also interesting to check the magnitude of correction coming from the fact that real neurons are not equipotential and action potentials propagate and back-propagate with a finite velocity. Let ζ be the spatial constant characterizing membrane potential homogeneity, and c the velocity of action potential propagation (along axon) and back-propagation (along dendrites). A simple way to account for the spatio-temporal dependence of Na^+ conductance and voltage in Eq. (25) is to make the following rescalings:

$$g_{Na}(x, t) \approx \bar{g}_{Na}(1 - (t - x/c)/\tau_o) \exp(-(ct - x)/\zeta) H(ct - x) H(x + c\tau_o - ct)$$

and

$$V(x, t) \approx \{V_{Na}(1 - (t - x/c)^z/\tau_o^z) \exp(-(ct - x)/\zeta) + 0.6V_K(t - x/c)^z/\tau_o^z\} H(ct - x) H(x + c\tau_o - ct),$$

where the factor $\exp(-(ct - x)/\zeta)$ denotes a traveling wave of excitation along axon or dendrite with the spatial spread ζ , and the function $H(y)$ is the standard Heaviside function equal to 1 for $y \geq 0$ and equal to 0 for $y < 0$. These rescalings assure that points along axon and dendrite separated by x from the soma (action potential initiation zone) receive an excitation after the delay time x/c . With these modifications, after some algebra, the corrected result for the $\Delta[\text{Na}]_o^{(2)}$ is

$$\Delta[\text{Na}]_o^{(2)} \approx \frac{4\bar{g}_{Na}\tau_o(V_{Na} - 0.6V_K)}{Fd(z+1)(z+2)} \left(1 + \epsilon \frac{c\tau_o}{\zeta}\right), \quad (27)$$

where ϵ is given by $\epsilon = \frac{(z+1)}{(V_{Na}-0.6V_K)} \{(z+2)V_{Na}/6 - (2V_{Na} - 0.6V_K)/(z+3)\}$. The term proportional to $c\tau_o/\zeta$ represents the first order correction and it is clear that the

equipotential approximation corresponds to the case when $\zeta = \infty$ or $c\tau_o/\zeta \ll 1$. For physiological values of parameters: $V_{Na} = 60$ mV, $V_K = -100$ mV, $c = 2.3$ mm/msec, $\zeta = 1$ mm (Koch, 1998), with $\tau_o = 0.4$ msec and $z = 2.5$, we obtain $\epsilon c\tau_o/\zeta \approx 0.22$. This implies that the equipotential assumption slightly underestimates the sodium influx during the second phase of sodium activation. Overall, this correction to the total Na^+ influx $\Delta[\text{Na}]_o$ is small, $\sim 16\%$, for low firing rates for which $\delta C \approx 2.4C$, and it gets even smaller for high firing rates. A detailed numerical treatment of the influence of action potential velocity on metabolic rate of the squid giant axon is presented in (Crotty et al, 2006).

Appendix B: Relaxation time constant for Na^+ dynamics.

In this Appendix the relaxation process of voltage and sodium to their equilibrium values is analyzed following a single action potential for a neuron that prior to that has been at rest for a long time. Computations below are performed in a very late phase of an action potential when the conductances g_{Na} , g_K , and the voltage V returned essentially to their resting values (or are close to them, i.e. $dV/dt \approx 0$). During this phase we can use a linear approximation on V and $[\text{Na}]$ in Eq. (6). That is, we can expand V and $[\text{Na}]$ around their resting values V_o and $[\text{Na}]_o$ as: $V \approx V_o + \Delta V$, $[\text{Na}] \approx [\text{Na}]_o + \Delta[\text{Na}]$, where $\Delta[\text{Na}]/[\text{Na}]_o \ll 1$, and neglect higher order terms. In this approximation the pump current I_p can be written as $I_p \approx I_{p,o} + \lambda\Delta[\text{Na}]$, where $I_{p,o} = AS[\text{Na}]_o^k/([\text{Na}]_o^k + \theta^k)$, and $\lambda = kA\theta^k[\text{Na}]_o^{k-1}/(\theta^k + [\text{Na}]_o^k)^2$. The corresponding changes in V_{Na} and V_K are $\Delta V_{Na} \approx -(RT/F)\Delta[\text{Na}]/[\text{Na}]_o$ and $\Delta V_K \approx -(RT/F)\Delta[\text{K}]/[\text{K}]_o = (RT/F)\Delta[\text{Na}]/[\text{K}]_o$.

Next, using the facts that $g_{Na}/g_L \ll 1$ and $g_K/g_L \ll 1$, we can solve Eq. (6) analytically.

The equations governing $\Delta[\text{Na}]$ and ΔV relaxations are given by:

$$\begin{aligned} \frac{dF}{4} \frac{d}{dt} \Delta[\text{Na}] &= - \left\{ 3\lambda + \frac{RT}{F[\text{Na}]_o} \left(g_{Na} - \frac{qf\rho_s d g_s \tau_s V_K (V_o - V_K)}{4(1-\phi)(V_K - V_{Na})^2} \right) \right\} \Delta[\text{Na}] \\ \Delta V(t) &\approx - \frac{\{\lambda + (RT/F)(g_{Na}/[\text{Na}] - g_K/[\text{K}])\} \Delta[\text{Na}]}{\{g_L + qf\rho_s g_s \tau_s d / (4(1-\phi))\}}. \end{aligned} \quad (28)$$

The term on the right hand side of $\Delta[\text{Na}]$ dynamics that is proportional to $RT/(F[\text{Na}]_o)$ is much smaller than 3λ , and thus it can be neglected. This implies that changes in V_{Na} and V_K due to sodium influx for an isolated action potential are very small. This leads to a simple exponential decay of $\Delta[\text{Na}]$ as $\Delta[\text{Na}] \approx \Delta[\text{Na}]_o e^{-t/\tau}$ with the time constant $\tau \approx Fd/(12\lambda)$, where $\Delta[\text{Na}]_o$ is Na^+ influx during the action potential given by Eq. (12). Thus, relaxation time constant is short for thin fibers, and it increases proportionally with fiber diameter. As an example, for $d = 0.45 \mu\text{m}$ we obtain $\tau \approx 5$ sec (for $k = 3$ and $[\text{Na}]_o = 12.0$), which is of the right order of magnitude (Abercrombie and Weer, 1978; Nakao and Gadsby, 1989). For $d = 0.18 \mu\text{m}$ the time constant τ is about 2 sec.

Appendix C: Solution of the thermal balance equation.

The steady-state limit of Eq. (9) can be rewritten in the form:

$$\frac{\partial^2 T}{\partial r^2} = \frac{\rho_{bl} c_{bl} \text{CBF}}{\kappa} (T - T_o), \quad (29)$$

where $T_o = T_{bl} + G_{ATP}/(\rho_{bl}c_{bl}CBFU_{br})$. In computations, we assume $G_{ATP} \approx P_{ATP}$ because of the high efficiency of Na^+/K^+ -ATPase (Sec. 3.5). We look for the solution of Eq. (29) in the form: $T(r) = T_o + a \exp(\xi r)$. Substituting this form in Eq. (29), we obtain $\xi = \pm(\rho_{bl}c_{bl}CBF/\kappa)^{1/2}$, and we take only the positive solution as the one corresponding to the physical situation. From the boundary condition in Eq. (10) we obtain the coefficient $a = -\{\sigma_{SB}(T_{sc}^4 - T_o^4) + \eta(T_{sc} - T_o)\} e^{-\xi R}/(\kappa\xi)$. Combining these results we find Eq. (21) in the main text. The scalp temperature T_{sc} is determined numerically from the condition $T_{sc} = T(R)$, for all considered species.

References

- Abercrombie RF, De Weer P (1978) Electric current generated by squid giant axon sodium pump: external K and internal ADP effects. *Am. J. Physiol.* **235**: C63-C68.
- Aiello LC, Wheeler P (1995) The expensive-tissue hypothesis: the brain and the digestive-system in human and primate evolution. *Curr. Anthropol.* **36**: 199-221.
- Ames III A (2000) CNS energy metabolism as related to function. *Brain Research Reviews* **34**: 42-68.
- Amir Y, Harel M, Malach R (1993) Cortical hierarchy reflected in the organization of intrinsic connections in macaque monkey visual cortex. *J. Comp. Neurol.* **334**: 19-46.
- Astrup J, Sorensen PM, Sorensen HR (1981) Oxygen and glucose consumption related to Na^+ - K^+ transport in canine brain. *Stroke* **12**: 726-730.
- Attwell D, Laughlin SB (2001) An energy budget for signaling in the gray matter of the brain. *J. Cereb. Blood Flow Metabol.* **21**: 1133-1145.
- Baddeley R, et al (1997) Responses of neurons in primary and inferior temporal visual cortices to natural scenes. *Proc. R. Soc. Lond. B* **264**: 1775-1783.
- Baker MA (1982) Brain cooling in endotherms in heat and exercise. *Annu. Rev. Physiol.* **44**: 85-96.
- Bennett CH (1982) The thermodynamics of computation - a review. *Int. J. Theor. Physics* **21**: 905-940.
- Braendgaard H, et al (1990) The total number of neurons in the human neocortex unbiasedly estimated using optical disectors. *J. Microsc.* **157**: 285-304.
- Braitenberg V, Schüz A (1998) *Cortex: Statistics and Geometry of Neuronal Connec-*

tivity. Berlin: Springer.

Busija DW (1984) Sympathetic nerves reduce cerebral blood flow during hypoxia in awake rabbits. *Am. J. Physiol.* **247**: H446-H451.

Cherniak C (1995) Neural component placement. *Trends Neurosci.* **18**: 522-527.

Chklovskii DB, Schikorski T, Stevens CF (2002) Wiring optimization in cortical circuits. *Neuron* **43**: 341-347.

Clarke DD, Sokoloff L, In "Basic Neurochemistry", ed: Siegel GJ et al (New York, Raven Press, 1994), pp. 645-680.

Cragg BG (1967) The density of synapses and neurones in the motor and visual areas of the cerebral cortex. *J. Anatomy* **101**: 639-654.

Craig AD (2003) Interoception: the sense of the physiological condition of the body. *Curr. Opin. Neurobiol.* **13**: 500-505.

Crotty P, Sangrey T, Levy WB (2006) Metabolic energy cost of action potential velocity. *J. Neurophysiol.* **96**: 1237-1246.

Dayan P, Abbott LF (2001). *Theoretical Neuroscience*. Cambridge, MA: MIT Press.

DeFelipe, J., Alonso-Nanclares, L., and Avellano, J (2002) Microstructure of the neocortex: Comparative aspects. *J. Neurocytology* **31**: 299-316.

Erecinska M, Silver IA (1989) ATP and brain function. *J. Cereb. Blood Flow Metab.* **9**: 2-19.

Faisal AA, White JA, Laughlin SB (2005) Ion-channel noise places limits on the miniaturization of the brain's wiring. *Curr. Biol.* **15**: 1143-1149.

Falk D (1990) Brain evolution in Homo: the "radiator" theory. *Behav. Brain. Sci.* **13**:

333-381.

Frietsch T et al (2007) Reduced cerebral blood flow but elevated cerebral glucose metabolic rate in erythropoietin overexpressing transgenic mice with excessive erythrocytosis. *J. Cereb. Blood Flow Metabol.* **27**: 469-476.

Gordon CJ (1993) *Temperature regulation in laboratory rodents*. Cambridge, UK: Cambridge Univ. Press.

Hayward JN, Baker MA (1968) Role of cerebral arterial blood temperature in the regulation of brain temperature in the monkey. *Am. J. Physiol.* **215**: 389-403.

Haug H (1987) Brain sizes, surfaces, and neuronal sizes of the cortex cerebri: A stereological investigation of Man and his variability and a comparison with some mammals (primates, whales, marsupials, insectivores, and one elephant). *Am. J. Anatomy* **180**: 126-142.

Hempleman SC, et al (2005) Spike firing allometry in avian intrapulmonary chemoreceptors: matching neural code to body size. *J. Exp. Biol.* **208**: 3065-3073.

Hensel H, Bruck K, Rath P (1973). *Homeothermic organisms*. In: *Temperature and Life*. Edited by: Precht H et al. New York: Springer-Verlag, p. 509-564.

Hille B (2001) *Ionic channels of excitable membranes*. Sunderland, MA: Sinauer Assoc., 3rd edition.

Hodgkin AL (1954) A note on conduction velocity. *J. Physiol.* **125**: 221-224.

Jansen MA et al (2003) Energy requirements for the Na⁺ gradient in the oxygenated isolated heart: effect of changing the free energy of ATP hydrolysis. *Am. J. Physiol. Heart Circ. Physiol.* **285**: H2437-H2445.

- Kaas JH (2000) Why is brain size so important: Design problems and solutions as neo-cortex gets bigger or smaller. *Brain Mind* **1**: 7-23.
- Kandel ER, Schwartz JH, Jessell TM (1991) *Principles of Neural Science*. Norwalk, Connecticut: Appleton and Lange, 3rd edition.
- Karbowski J (2001) Optimal wiring principle and plateaus in the degree of separation for cortical neurons. *Physical Review Letters* **86**: 3674-3677.
- Karbowski J (2003) How does connectivity between cortical areas depend on brain size? Implications for efficient computation. *J. Comput. Neurosci.* **15**: 347-356.
- Karbowski J (2007) Global and regional brain metabolic scaling and its functional consequences. *BMC Biology* **5**: 18.
- Kiyatkin EA (2007) Brain temperature fluctuations during physiological and pathological conditions. *Eur. J. Appl. Physiol.* **101**: 3-17.
- Koch C (1998) *Biophysics of computation*. Oxford: Oxford Univ. Press.
- Koehler RC, Traystman RJ, Jones MD (1985) Regional blood flow and O_2 transport during hypoxic and CO hypoxia in neonatal and adult sheep. *Am. J. Physiol.* **248**: H118-H124.
- Landauer R (1961) Irreversibility and heat generation in the computing process. *IBM J. Res. Dev.* **5**: 183-191.
- Lennie P (2003) The cost of cortical computation. *Curr. Biol.* **13**: 493-497.
- Linde R, Schmalbruch IK, Paulson OB, Madsen PL (1999) The Kety-Schmidt technique for repeated measurements of global cerebral blood flow and metabolism in the conscious rat. *Acta Physiol. Scand.* **165**: 395-401.

Madsen PL et al (1991) Cerebral O_2 metabolism and cerebral blood flow in humans during deep and rapid-eye-movement sleep. *J. Appl. Physiol.* **70**: 2597-2601.

Marcus ML, Heistad DD (1979) Effects of sympathetic nerves on cerebral blood flow in awake dogs. *Am. J. Physiol.* **236**: H549-H553.

Markram H et al (1997) Physiology and anatomy of synaptic connections between thick tufted pyramidal neurones in the developing rat neocortex. *J. Physiol.* **500**: 409-440.

Markram H, Wang Y, Tsodyks M (1998) Differential signaling via the same axon of neocortical pyramidal neurons. *Proc. Natl. Acad. Sci. USA* **95**: 5323-5328.

McElligott JG, Melzack R (1967) Localized thermal changes evoked in the brain by visual and auditory stimulation. *Exp. Neurol.* **17**: 293-312.

Murre JMJ, Sturdy DPF (1995) The connectivity of the brain: Multilevel quantitative analysis. *Biol. Cybern.* **73**: 529-545.

Nakao M, Gadsby DC (1989) [Na] and [K] dependence of the Na/K pump current-voltage relationship in guinea pig ventricular myocytes. *J. Gen. Physiol.* **94**: 539-565.

Nelson DA, Nunneley SA (1998) Brain temperature and limits on transcranial cooling in humans: quantitative modeling results. *Eur. J. Appl. Physiol.* **78**: 353-359.

Nybo L, Secher NH, Nielsen B (2002) Inadequate heat release from the human brain during prolonged exercise with hyperthermia. *J. Physiol.* **545**: 697-704.

Prothero (1997) Cortical scaling in mammals: A repeating units model. *J. Brain Res.* **38**: 195-207.

Purves D (1988) *Body and Brain*. Cambridge, Massachusetts: Harvard Univ. Press.

Raichle ME (2003) Functional brain imaging and human brain function. *J. Neurosci.*

23: 3959-3962.

Rolfe DFS, Brown GC (1997) Cellular energy utilization and molecular origin of standard metabolic rate in mammals. *Physiol. Rev.* **77**: 731-758.

Schmidt-Nielsen K (1984) *Scaling: Why is Animal Size so Important?* Cambridge: Cambridge Univ. Press.

Siesjo B (1978) *Brain Energy Metabolism*. New York: Wiley.

Stephan H, Baron G, Frahm HD (1981) New and revised data on volumes of brain structures in insectivores and primates. *Folia Primatol.* **35**: 1-29.

Stowe K (1984) *Introduction to Statistical Mechanics and Thermodynamics*. New York: Wiley.

Striedter GF (2005) *Principles of Brain Evolution*. Sunderland, MA: Sinauer Assoc.

Sukstanskii AL, Yablonskiy DA (2006) Theoretical model of temperature regulation in the brain during changes in functional activity. *Proc. Natl. Acad. Sci. USA* **103**: 12144-12149.

Traub R, Miles R (1991) *Neuronal Networks of the Hippocampus*. Cambridge, UK: Cambridge Univ. Press.

Waschke K et al (1993) Local cerebral blood flow and glucose utilization after blood exchange with a hemoglobin-based O_2 carrier in conscious rats. *Am. J. Physiol.* **265**: H1243-H1248.

van Leeuwen GMJ et al (2000) Numerical modeling of temperature distribution within the natal head. *Pediatr. Res.* **48**: 351-356.

Volgushev M, et al (2004) Probability of transmitter release at neocortical synapses at

different temperatures. *J. Neurophysiol.* **92**: 212-220.

Yablonskiy DA, Ackerman JJH, Raichle ME (2000) Coupling between changes in human brain temperature and oxidative metabolism during prolonged visual stimulation. *Proc. Natl. Acad. Sci. USA* **97**: 7603-7608.

Yoshinura Y, Kimura F, Tsumoto T (1999) Estimation of single channel conductance underlying synaptic transmission between pyramidal cells in the visual cortex. *Neuroscience* **88**: 347-352.

Zhang K, Sejnowski TJ (2000) A universal scaling law between gray matter and white matter of cerebral cortex. *Proc. Natl. Acad. Sci. USA* **97**: 5621-5626.

Figure Captions

Fig. 1

Heat transfer in the brain. Brain is represented as half of the ball with three concentric layers representing (from the brain outside): cerebrospinal fluid, skull, and scalp. The heat generated in the brain is removed by cerebral blood flow (small circles), conduction through the brain and three layers (dashed arrows), and scalp convection/conduction and radiation (dashed circular line).

Fig. 2

Sodium influx during an action potential. (A) Temporal dependence of Na^+ (solid line) and K^+ (dashed line) conductances and voltage (dashed-dotted line) during the action potential. (B) The correction δC as a function of intracellular sodium concentration. (C) Dependence of sodium influx $\Delta[\text{Na}]_o$ on the effective fiber diameter d coming from a numerical integration of Eq. (6). The least square fit (solid line) yields the relationship: $\Delta[\text{Na}]_o = 2.72 \cdot 10^{-5} d^{-0.974}$ mM, where d is in cm. This numerical fit practically confirms the theoretical dependence $\Delta[\text{Na}]_o \sim d^{-1}$ in Eq. (12).

Fig. 3

Dependence of the intracellular sodium concentration on time for a neuron firing repeatedly. (A) Results for $d = 0.45 \mu\text{m}$, i.e., the harmonic mean of the mouse axon diameter $d_a = 0.3 \mu\text{m}$ and dendrite diameter $d_d = 0.9 \mu\text{m}$ (see Sec. 2.2). (B) Results for $d = 0.11 \mu\text{m}$, i.e., for the smallest molecularly possible axons with $d_a = 0.06 \mu\text{m}$. Note that the range of variability in (B) is much larger, which reflexes higher amplitudes of Na^+ influx and its faster relaxation for thin fibers. Panels (A) and (B) come from

simulations of Eq. (6). (C) Simulation results for $d = 0.45 \mu\text{m}$ of Eq. (13) (solid lines) and its approximation Eq. (14) (dashed and dashed-dotted lines). For all plots in (A)-(C) $k = 3$.

Fig. 4

Intracellular sodium concentration as a function of firing rate. The point (diamonds) coming from a direct numerical integration of Eq. (6) are approximated well by the theoretical formula (15) (solid line). The maximal discrepancy for high frequency is about 15 – 20 %. The average $[\text{Na}]_{av}$ does not depend much on fiber diameter (panels A and C) nor on the Hill coefficient k (panels A and B).

Fig. 5

ATP and glucose utilization rates, and scaling of firing rate with brain size. (A) ATP rate increases non-linearly with frequency f and saturates for high values of f . (B) CMR_{glu} also increases non-linearly with firing rate, similar to the dependence of ATP on f . (C) Scaling of the estimated firing rates in mammals with brain size. The least square fit to the data points yields $f_{est} = 4.79U_g^{-0.15}$ Hz ($R^2 = 0.89$, $p = 0.0015$). Estimates of frequency are based on the empirical data of CMR_{glu} , which are (in $\mu\text{mol}/\text{cm}^3\text{min}$): 1.07 for mouse, 0.90 for rat, 0.83 for rabbit, 0.81 for cat, 0.47 for rhesus monkey, 0.46 for baboon, 0.34 for human. These data were taken from the data gathered in the supplementary information of Karbowski (2007). For all panels: $d = 0.45 \mu\text{m}$, $k = 3$.

Fig. 6

Dependence of the sodium pump power P_{ATP} on frequency and the effective fiber di-

ameter. (A) Biphasic dependence of P_{ATP} (per neuron per surface area) on frequency. Analytical formula (19) (solid line) leads to similar results as a direct numerical integration of Eq. (6) (diamonds). Results are for $d = 0.45 \mu\text{m}$. (B) P_{ATP} depends inversely on fiber diameter d . For extremely thin fibers P_{ATP} tends to diverge. Results are for $U_g = 680 \text{ cm}^3$ and $f = 1 \text{ Hz}$, corresponding to human brain. In both panels A and B, the Hill coefficient $k = 3$.

Fig. 7

Log-Log plot of the empirical dependence of the cerebral blood flow rate CBF on brain volume U_{br} for several mammals. The allometric dependence has the following form: $CBF = 0.018U_{br}^{-0.10} \text{ 1/sec}$, where U_{br} is expressed in cm^3 ($R^2 = 0.976$, $p = 0.0002$). The CBF empirical data are as follows: $20.2 \cdot 10^{-3} \text{ sec}^{-1}$ for mouse (Frietsch et al, 2007); $17.7 \cdot 10^{-3} \text{ sec}^{-1}$ for rat (Waschke et al, 1993; Linde et al, 1999); $14.3 \cdot 10^{-3} \text{ sec}^{-1}$ for rabbit (Busija, 1984); $12.7 \cdot 10^{-3} \text{ sec}^{-1}$ for dog (Marcus and Heistad, 1979); $10.7 \cdot 10^{-3} \text{ sec}^{-1}$ for sheep (Koehler et al, 1985); $9.2 \cdot 10^{-3} \text{ sec}^{-1}$ for human (Madsen et al, 1991). Brain volumes were taken from Stephan et al (1981) and Karbowski (2007).

Fig. 8

Brain temperature as a function of brain size, fiber diameter, and firing rate. (A) The spatial distribution of brain temperature $T(r)$. For very small brains $T(r)$ is smaller than the anterior blood temperature T_{bl} (dotted line). (B), (C) $T(0)$ strongly increases for very thin fibers ($U_g = 680 \text{ cm}^3$ corresponding to human brain for panel B and C; and $f = 1.7 \text{ Hz}$ for panel B). (D) Biphasic dependence of $T(0)$ on firing rate ($d = 0.45 \mu\text{m}$, $k = 3$). Solid line corresponds to human and dashed line to mouse.

Fig. 9

Lower bound on the effective fiber diameter d as a function of brain size and firing rate. (A) d_{min} depends very weakly on gray matter volume. (B) The lower bound on d_{min} depends biphasically on firing rate ($U_g = 680 \text{ cm}^3$). Weak synaptic depression ($\gamma = 0.1$; dashed line) leads to a similar dependence as moderate synaptic depression ($\gamma = 0.5$; solid line). The lower thermal bound on axon diameter d_a is approximately two times smaller than d_{min} , and therefore it is maximally $0.026 \mu\text{m}$.

Table 1: Parameters used in the article.

Parameter	Value	Units	Reference/Comment
$g_{Na,o}$	$2.9 \cdot 10^{-7}$	$(\Omega\text{cm}^2)^{-1}$	at -67 mV Traub-Miles model (1991)
$g_{K,o}$	$1.2 \cdot 10^{-6}$	$(\Omega\text{cm}^2)^{-1}$	at -67 mV Traub-Miles model (1991)
\bar{g}_{Na}	0.1	$(\Omega\text{cm}^2)^{-1}$	Traub-Miles model (1991)
\bar{g}_K	0.085	$(\Omega\text{cm}^2)^{-1}$	Traub-Miles model (1991)
g_L	10^{-4}	$(\Omega\text{cm}^2)^{-1}$	Traub-Miles model (1991)
g_s	$0.3 \cdot 10^{-9}$	Ω^{-1}	Yoshimura et al (1999)
q_0	0.17	unitless	Volgushev et al (2004) Markram et al (1998) Yoshimura et al (1999)
V_s	0.000	V	Koch (1998)
C	10^{-6}	F/cm ²	generally accepted
τ_s	$2.2 \cdot 10^{-3}$	sec	Koch (1998)
τ_d	0.5	sec	Dayan and Abbott (2001)
γ	0.5	unitless	Dayan and Abbott (2001)
A	$2 \cdot 10^{-6}$	A/cm ²	Abercrombie and De Weer (1978) Nakao and Gadsby (1989)
ρ_s	$5 \cdot 10^{11}$	cm ⁻³	Braitenberg and Schuz (1998) Craig (1967) DeFelipe et al (2002)
ϕ	1/3	unitless	Braitenberg and Schuz (1998)
F	96485.3	C/mol	Faraday constant
κ	$5 \cdot 10^{-3}$	W/(cm K)	van Leeuwen et al (2000)
σ_{SB}	$5.67 \cdot 10^{-12}$	W/(cm ² K ⁴)	Stowe (1984)
η	$1.2 \cdot 10^{-3}$	W/(cm K)	Nelson and Nunneley (1998) van Leeuwen et al (2000)
c_{bl}	$3.8 \cdot 10^3$	J/(kg K)	generally accepted
ρ_{bl}	$1.06 \cdot 10^{-3}$	kg/cm ³	generally accepted
T_{bl}	309.8	K	cerebral blood (body) temperature
T_o	293.2	K	room temperature (20 °C)

Table 2: Estimated neural activities and thermal brain properties in several mammals.

Species	f (Hz)	P_{ATP} (W)	$T(0)$ ($^{\circ}\text{C}$)	T_{sc} ($^{\circ}\text{C}$)	\dot{Q}_{bl} (W)	\dot{Q}_c (W)	\dot{Q}_{cv} (W)	\dot{Q}_r (W)
Mouse	6.18	0.003	36.57	35.5	-0.024	0.027	0.017	0.009
Rat	5.03	0.008	36.69	35.4	-0.058	0.066	0.043	0.022
Rabbit	4.59	0.054	36.81	35.3	-0.199	0.25	0.167	0.086
Cat	4.47	0.27	36.85	35.2	-0.51	0.78	0.51	0.26
Macaque	2.38	0.53	36.76	35.0	-1.25	1.78	1.18	0.60
Baboon	2.33	0.84	36.76	35.0	-1.65	2.49	1.64	0.84
Human	1.68	5.41	36.73	34.7	-6.02	11.43	7.55	3.88

In estimations it was assumed that blood temperature $T_{bl} = 36.6$ $^{\circ}\text{C}$, and it is brain size independent. The following values of gray matter volume U_g were used: 0.11 cm^3 for mouse; 0.42 cm^3 for rat; 3.0 cm^3 for rabbit; 15.2 cm^3 for cat; 50.0 cm^3 for macaque monkey; 80.0 cm^3 for baboon; and 680.0 cm^3 for human.

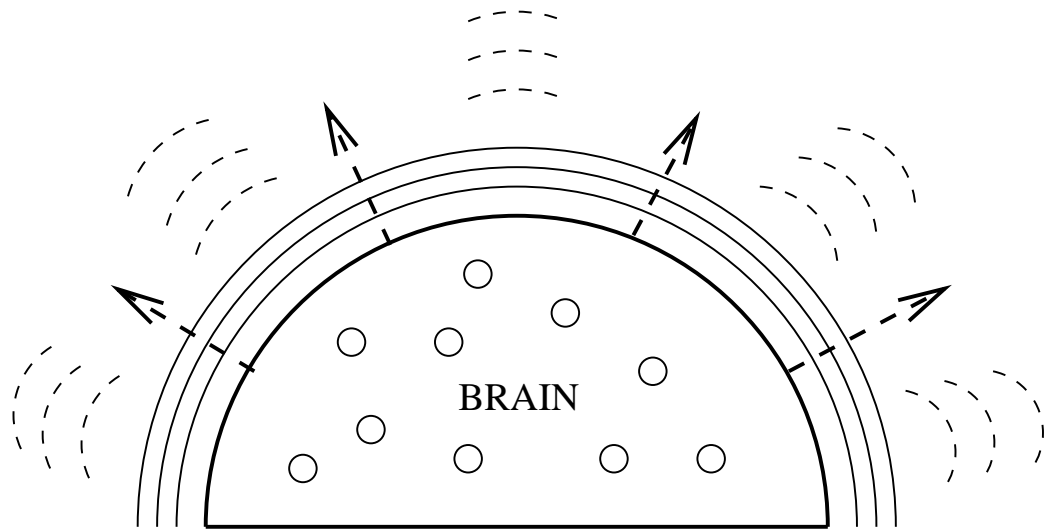


Figure 1

Figure 2A

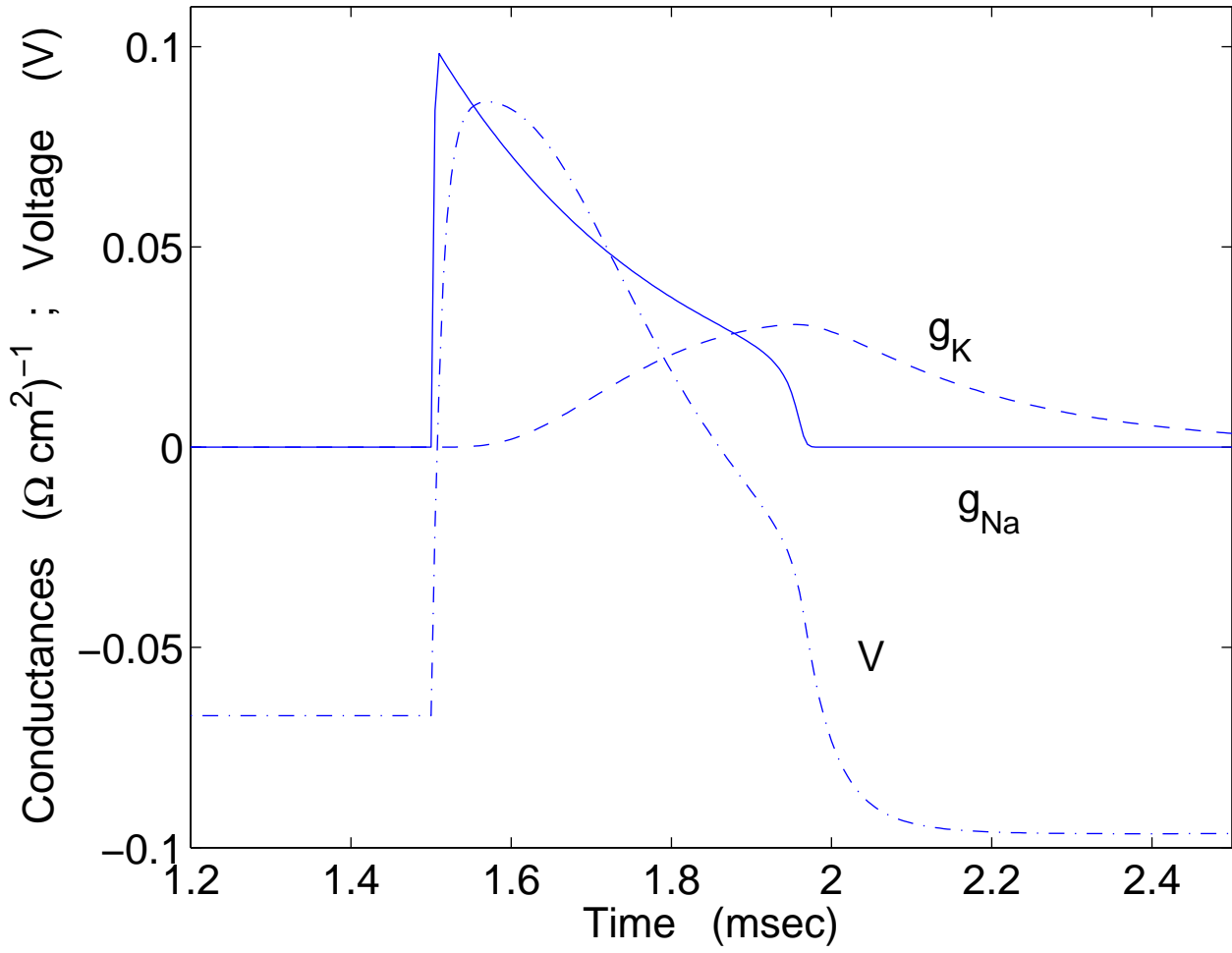


Figure 2B

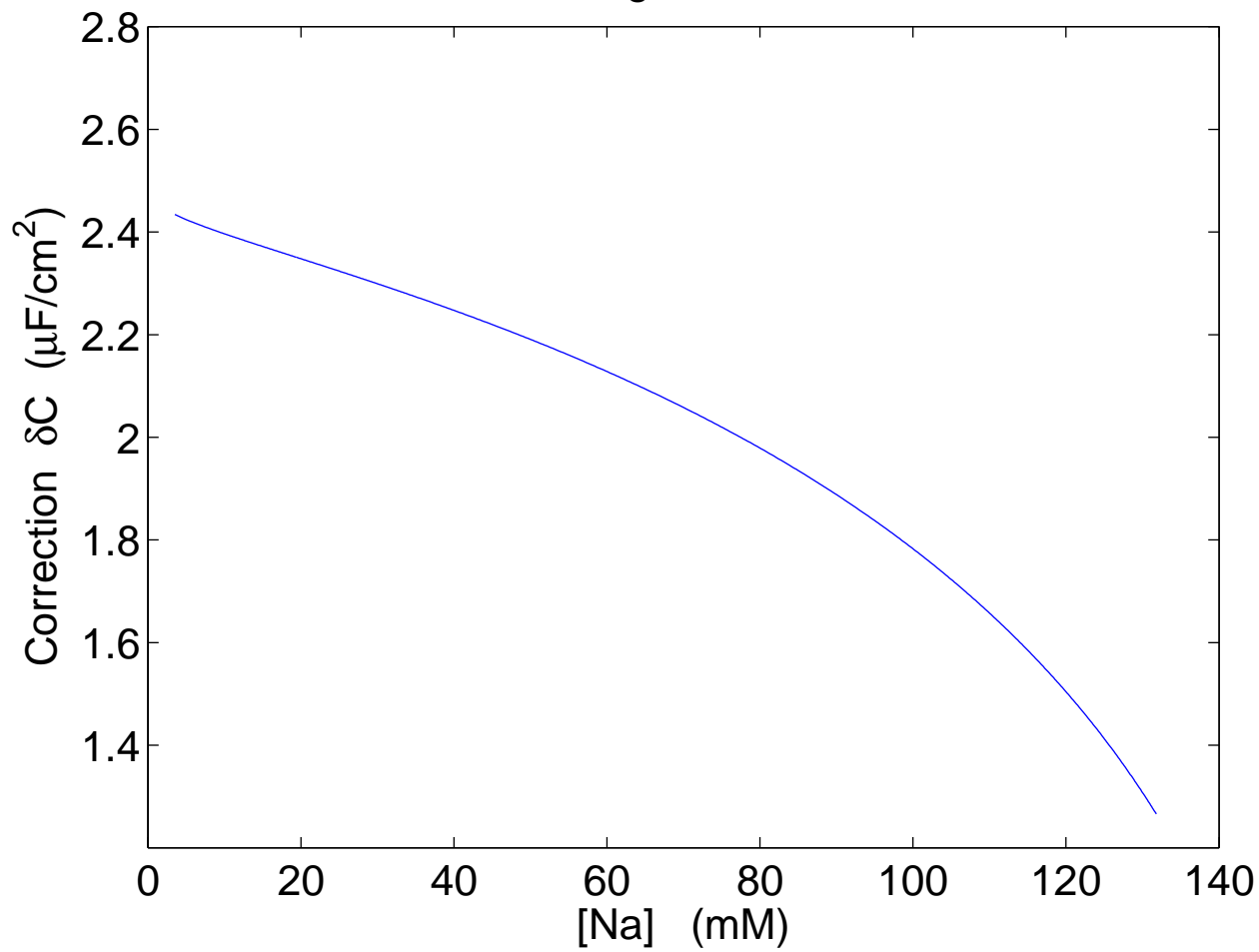


Figure 2C

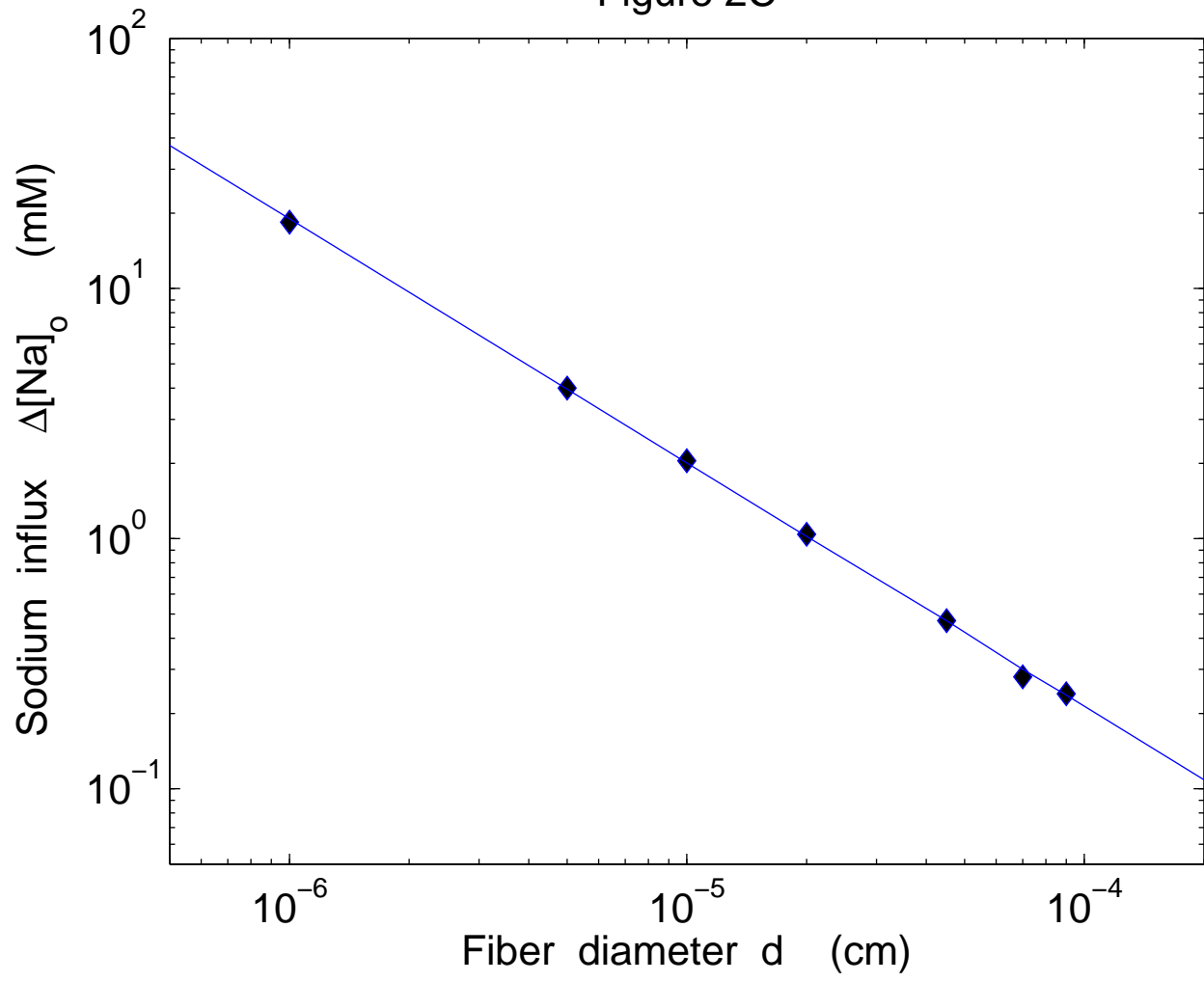


Figure 3A

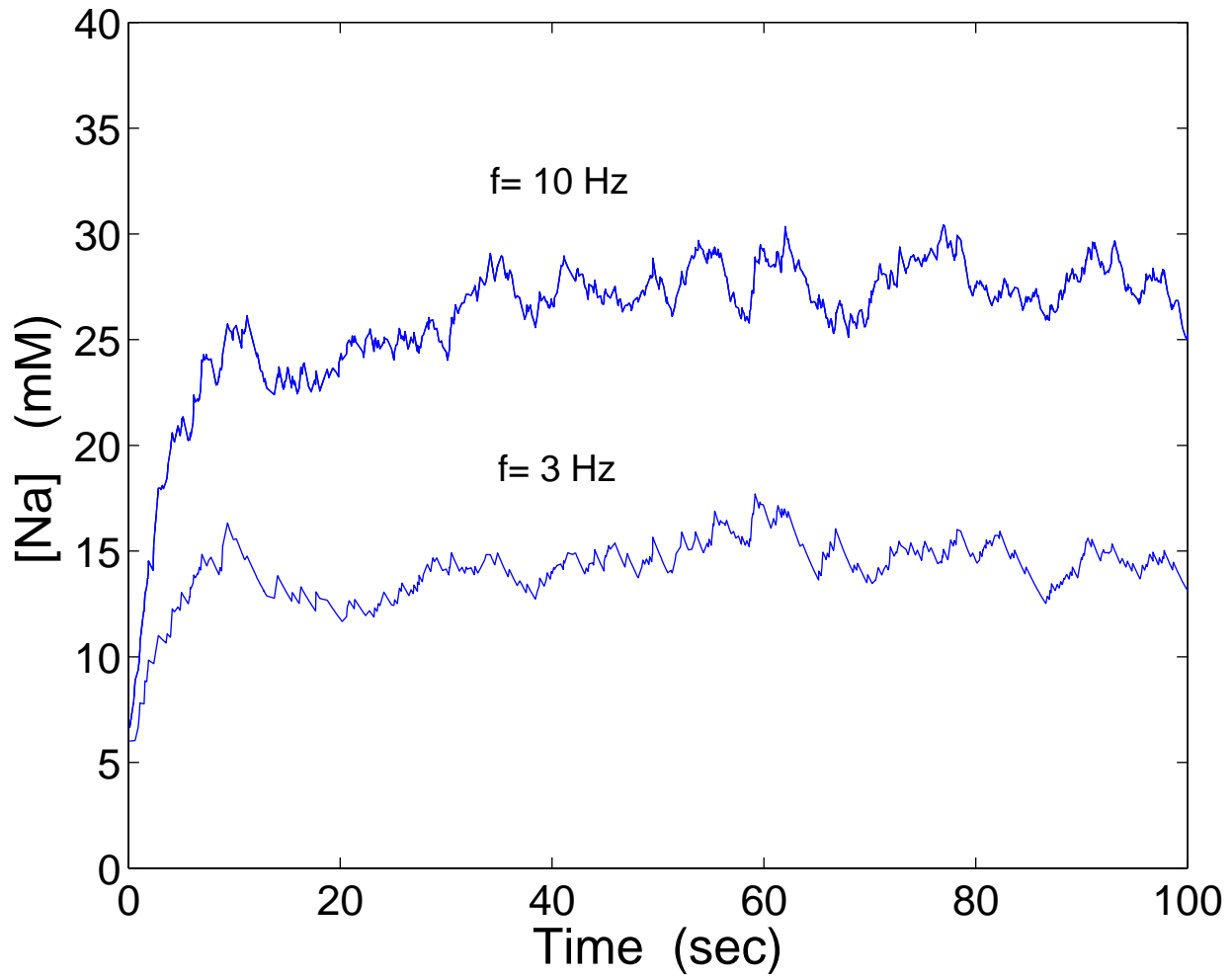


Figure 3B

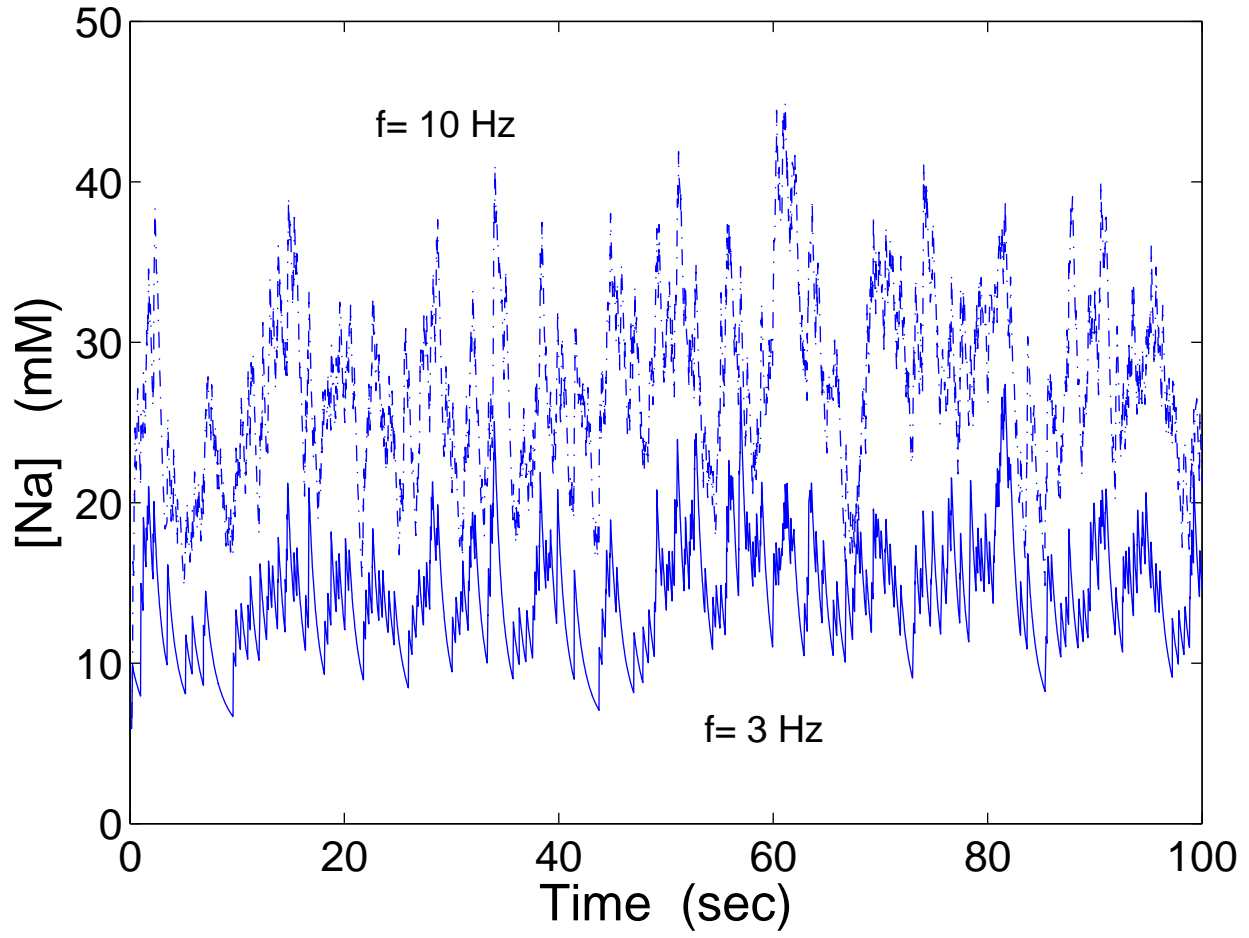


Figure 3C

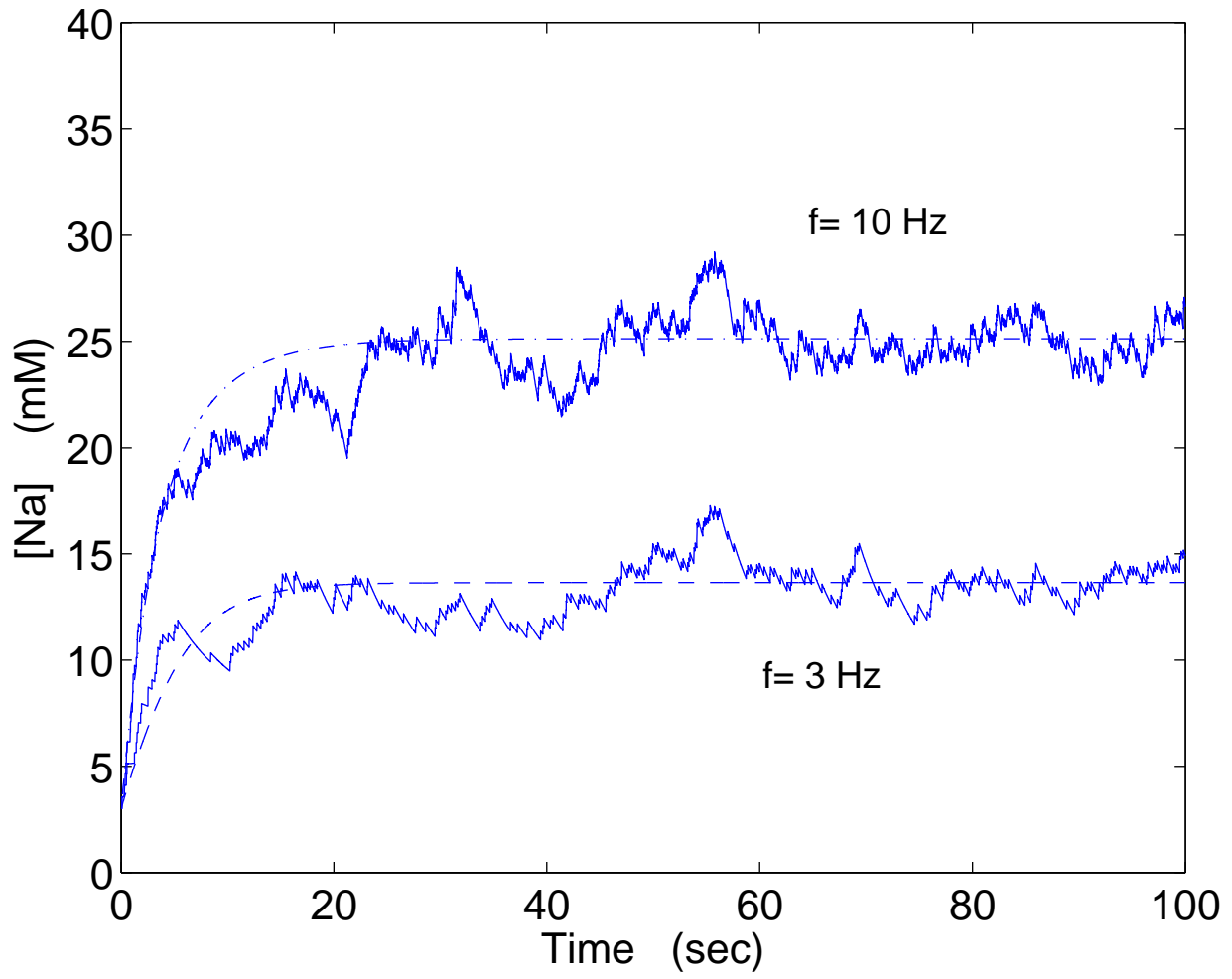


Figure 4A

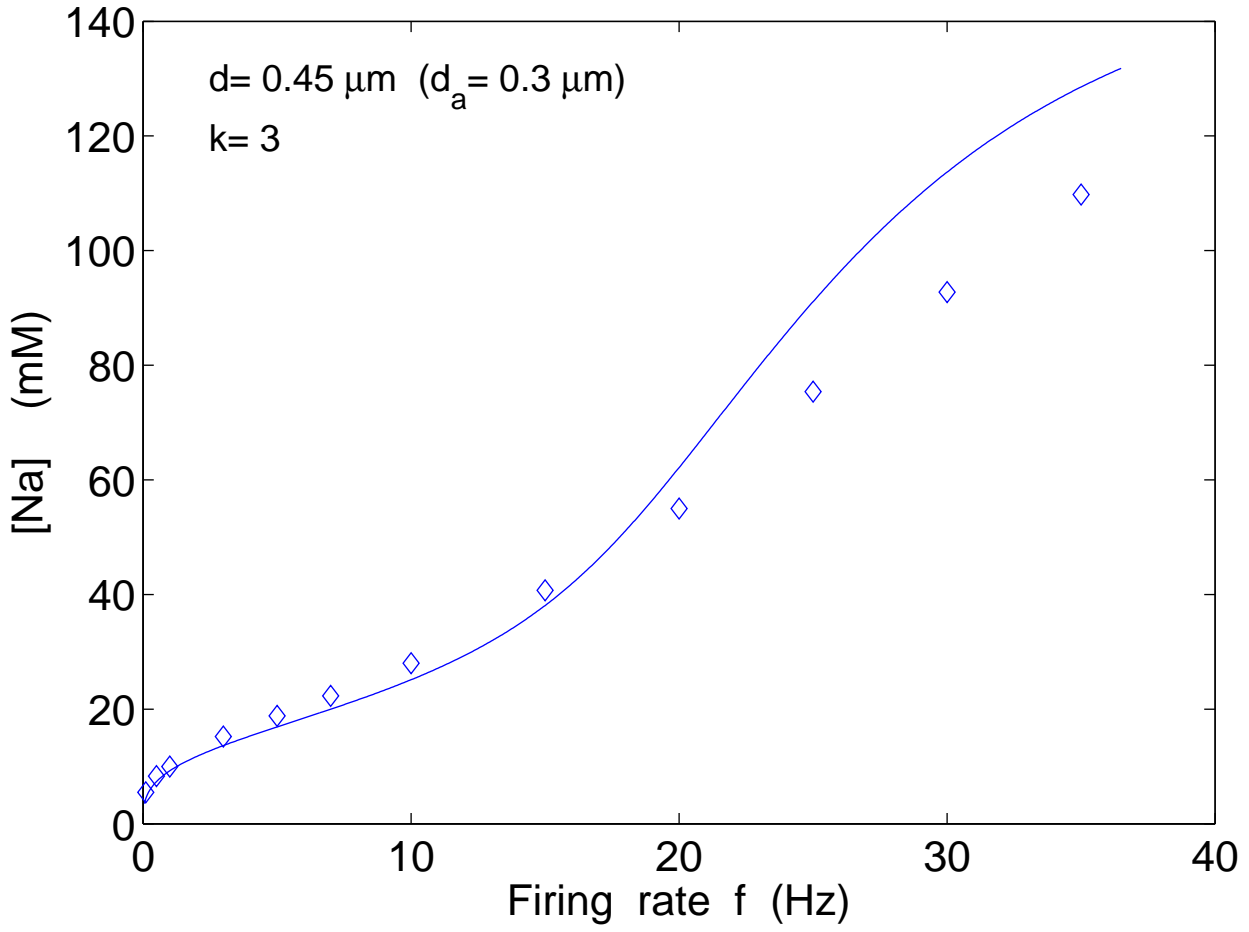


Figure 4B

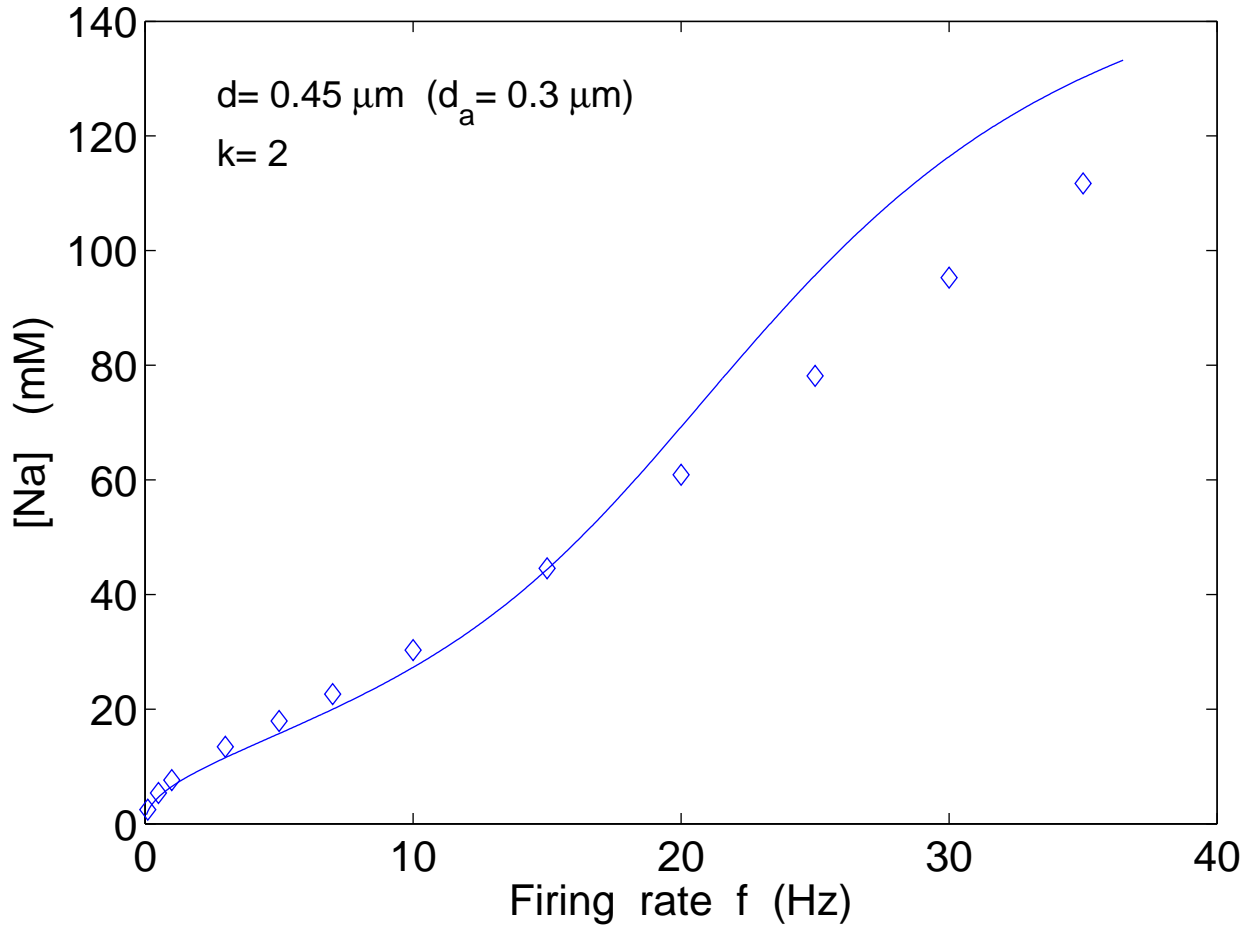


Figure 4C

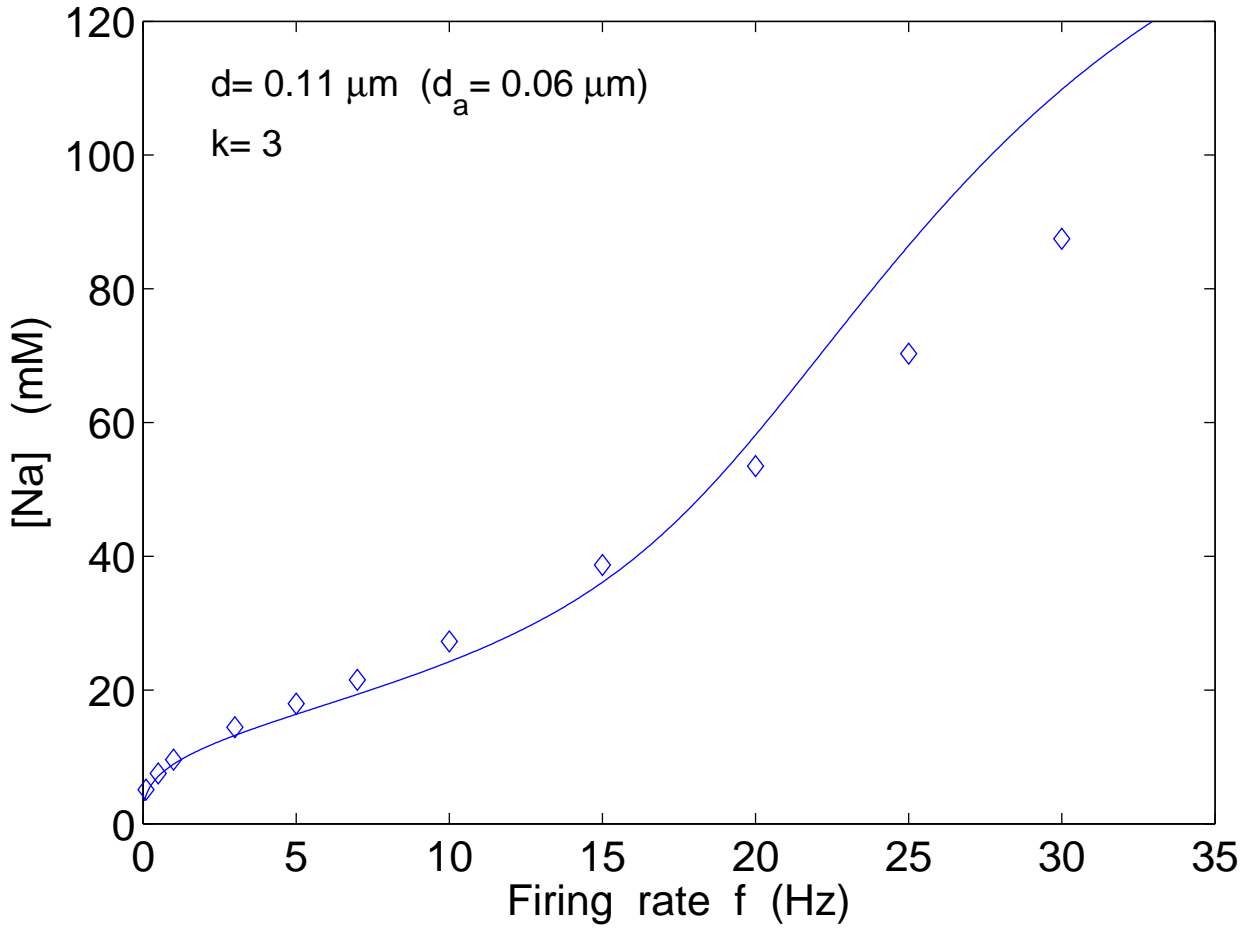


Figure 5A

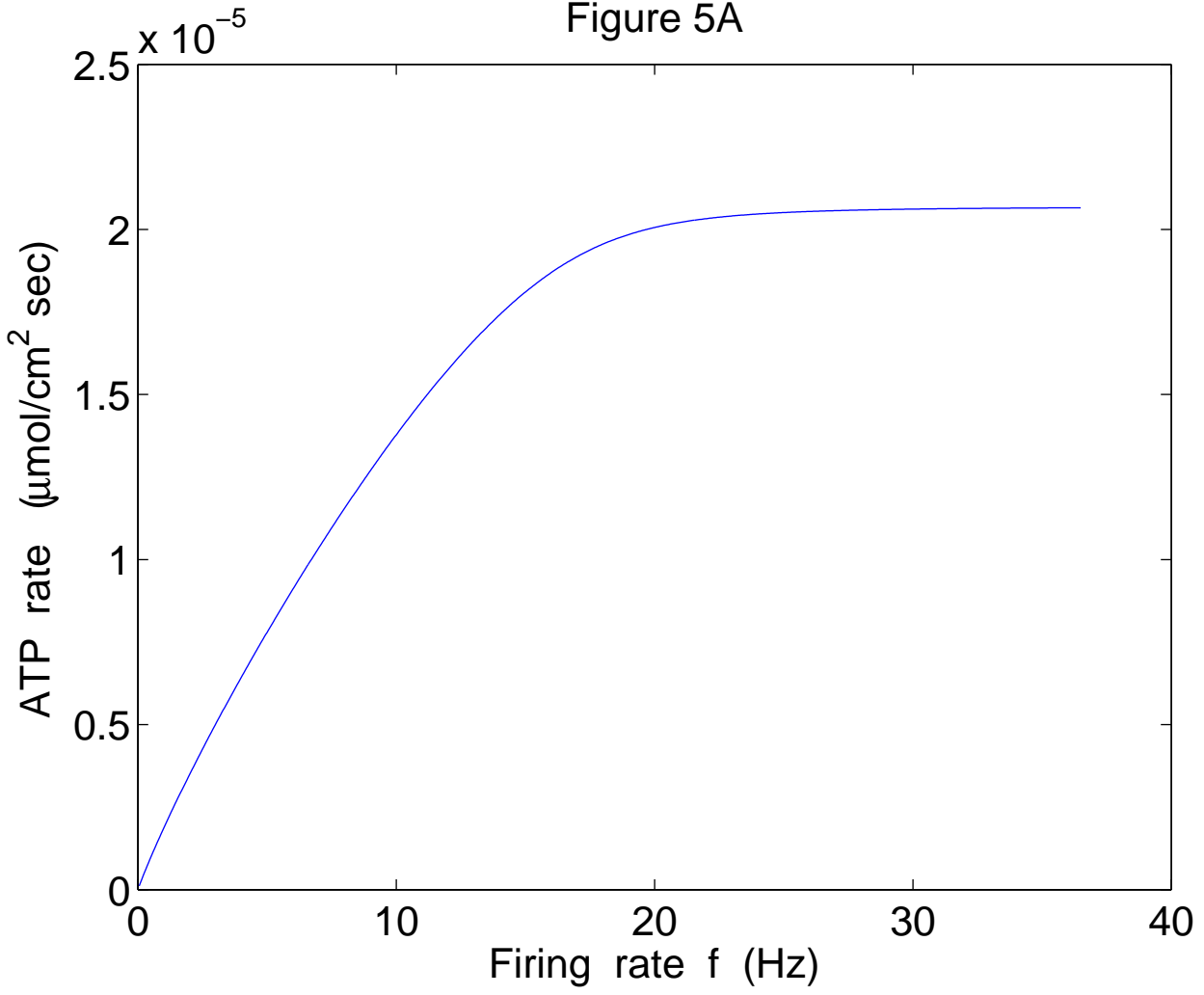


Figure 5B

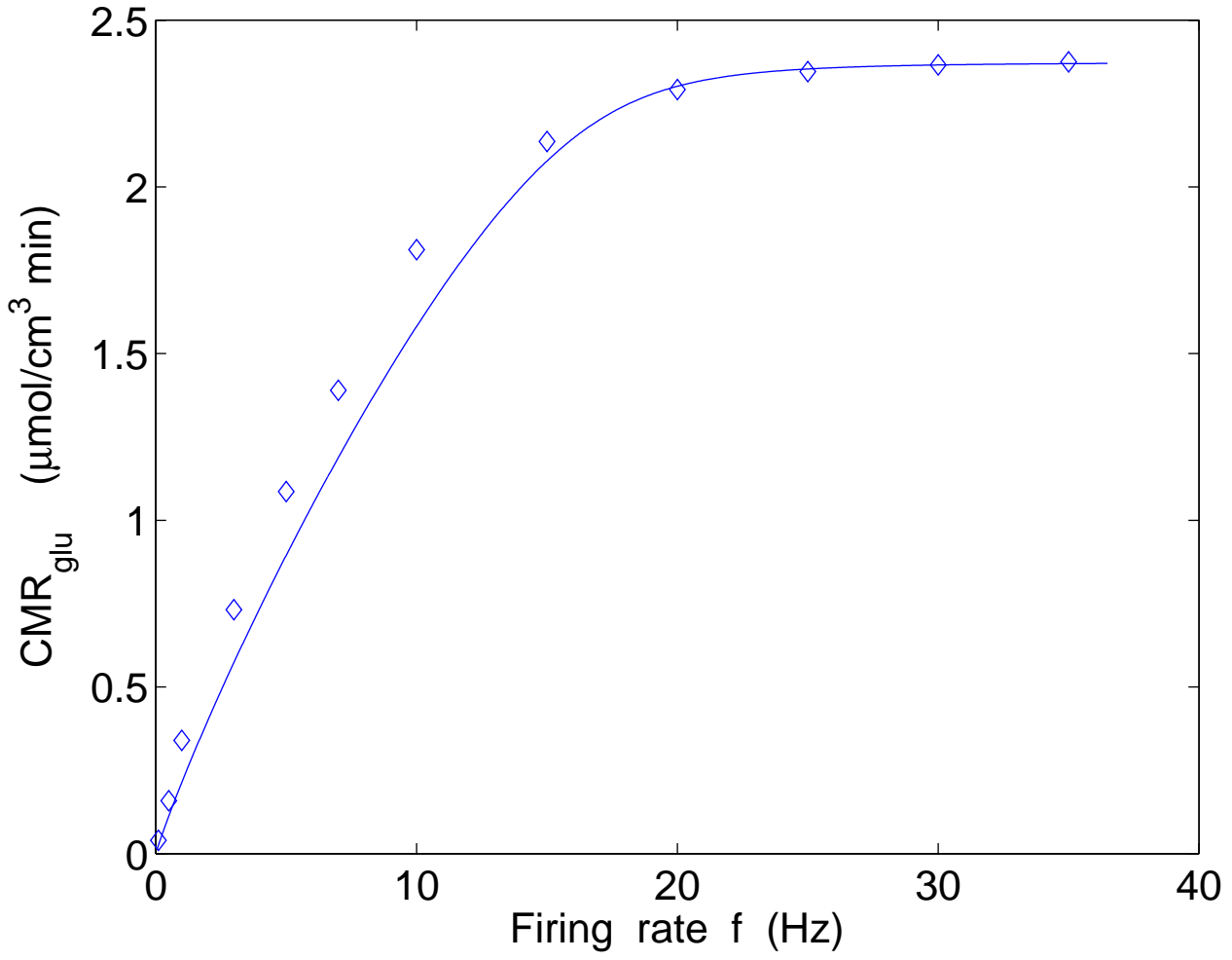


Figure 5C

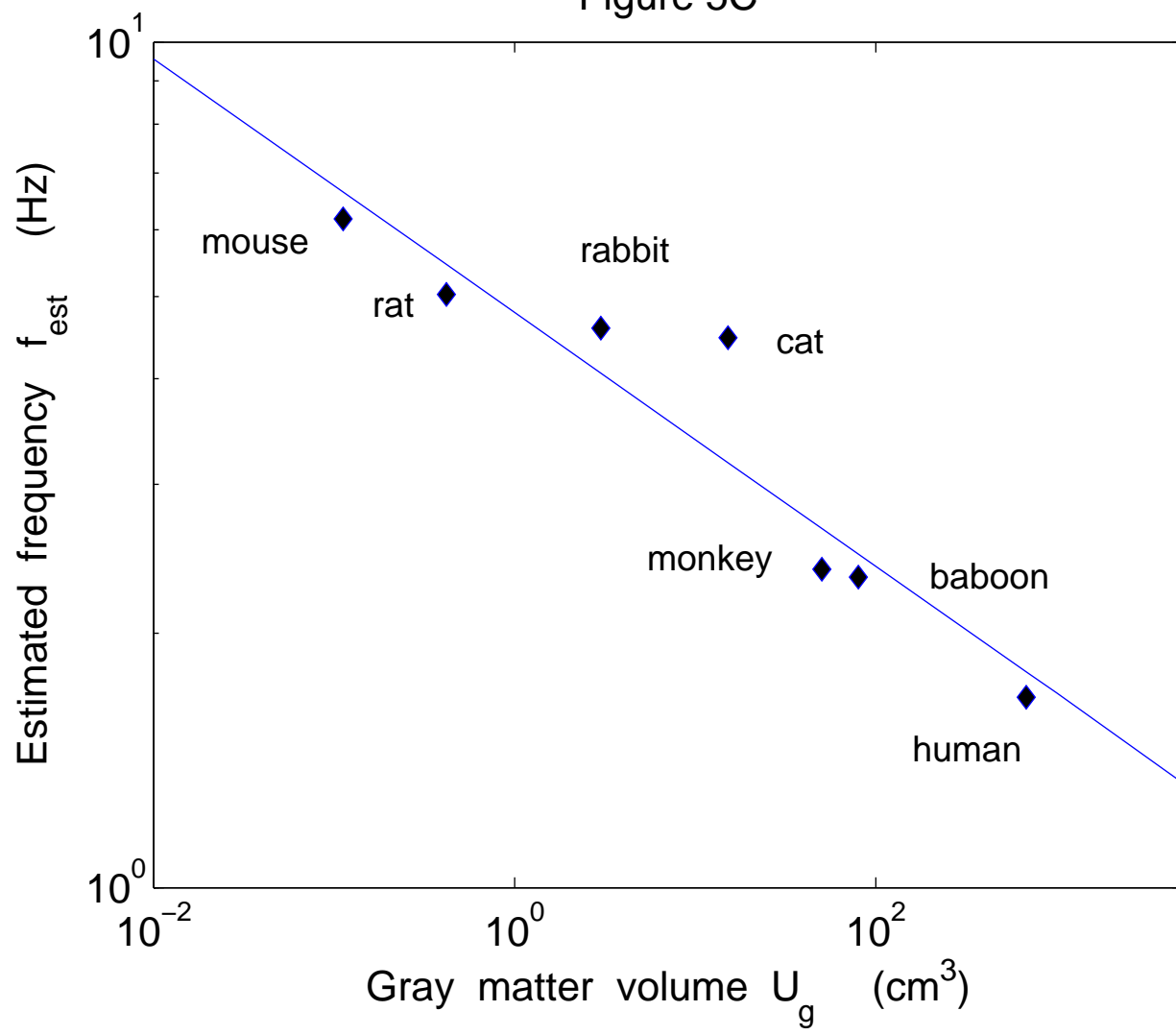


Figure 6A

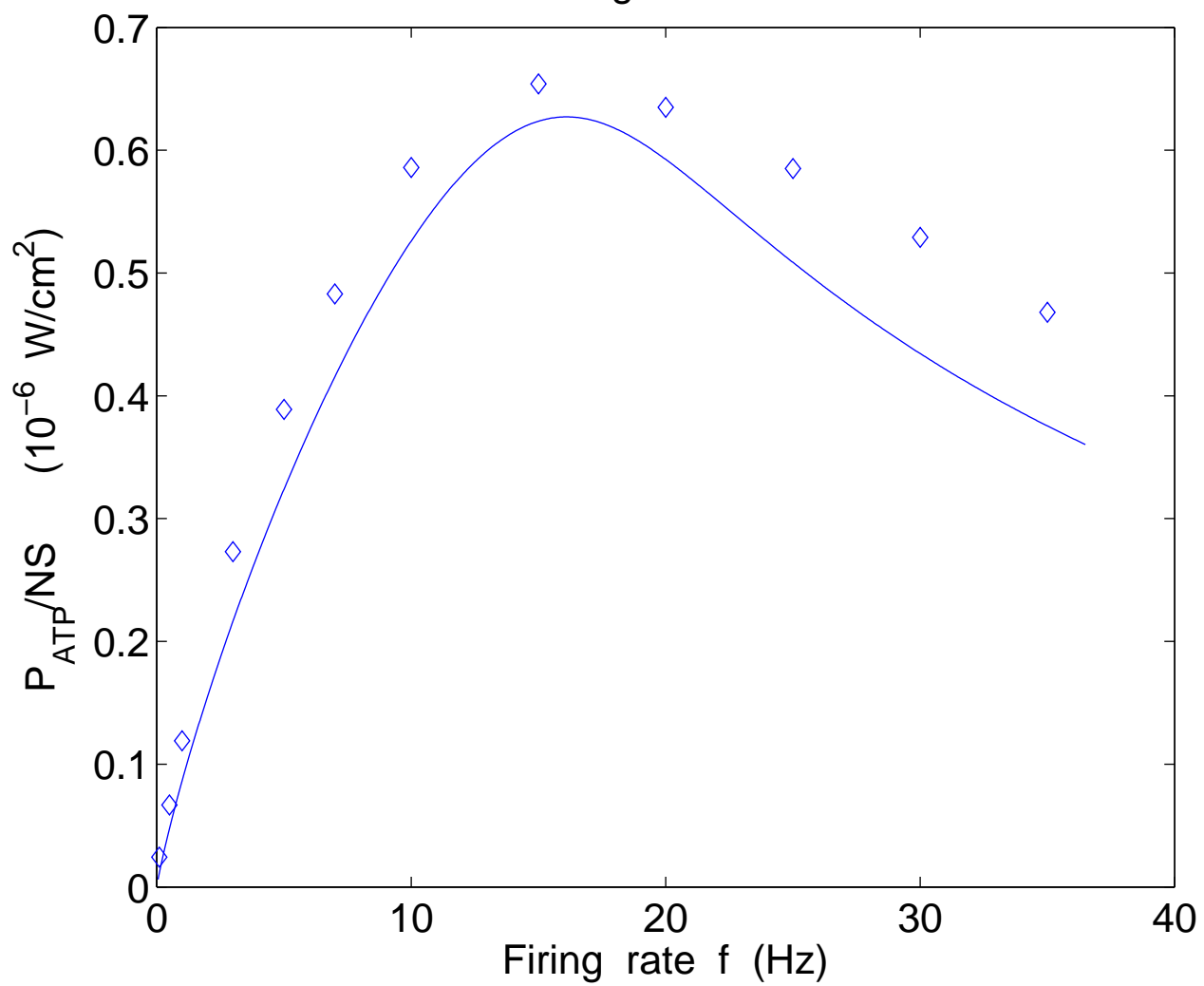


Figure 6B

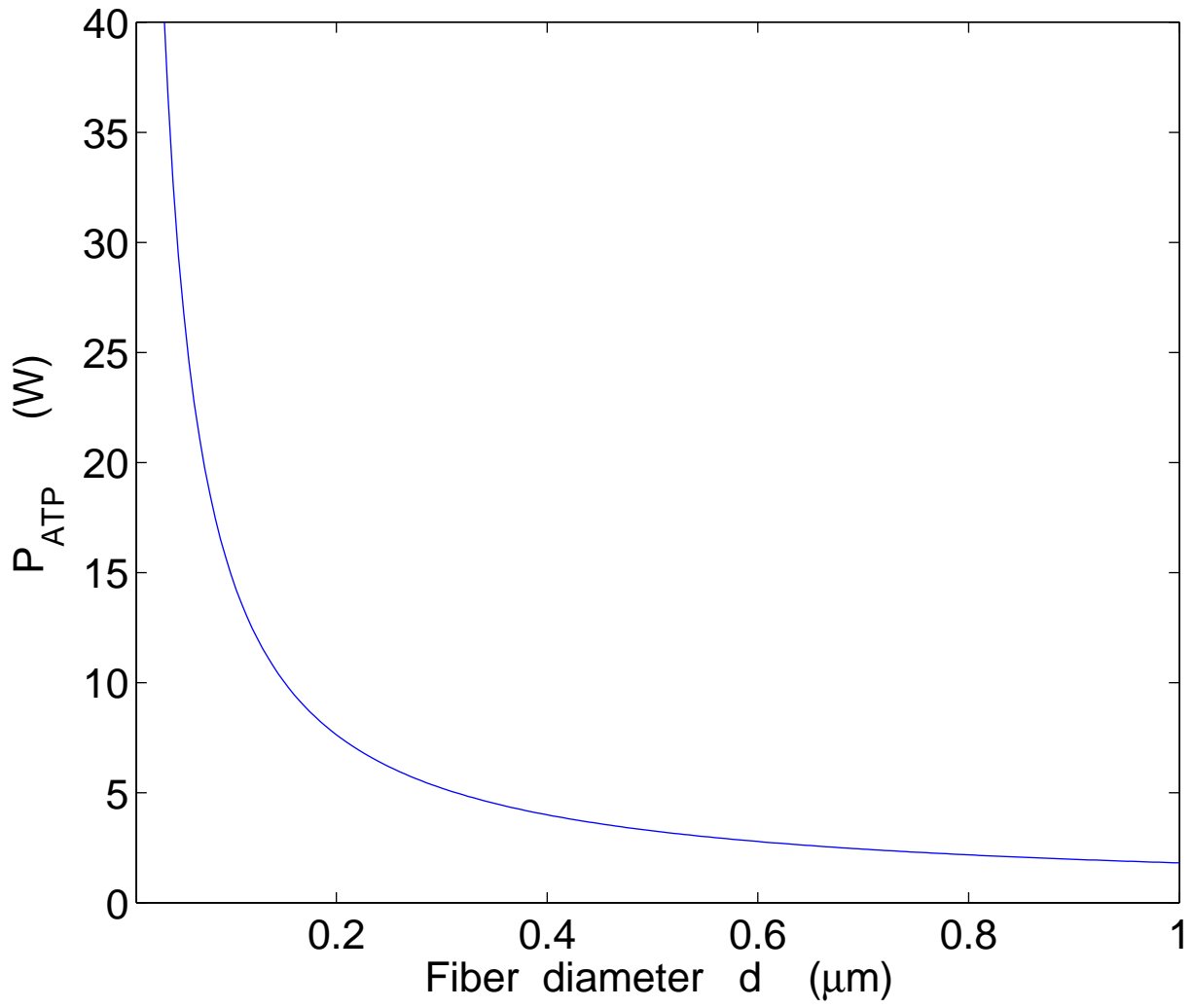


Figure 7

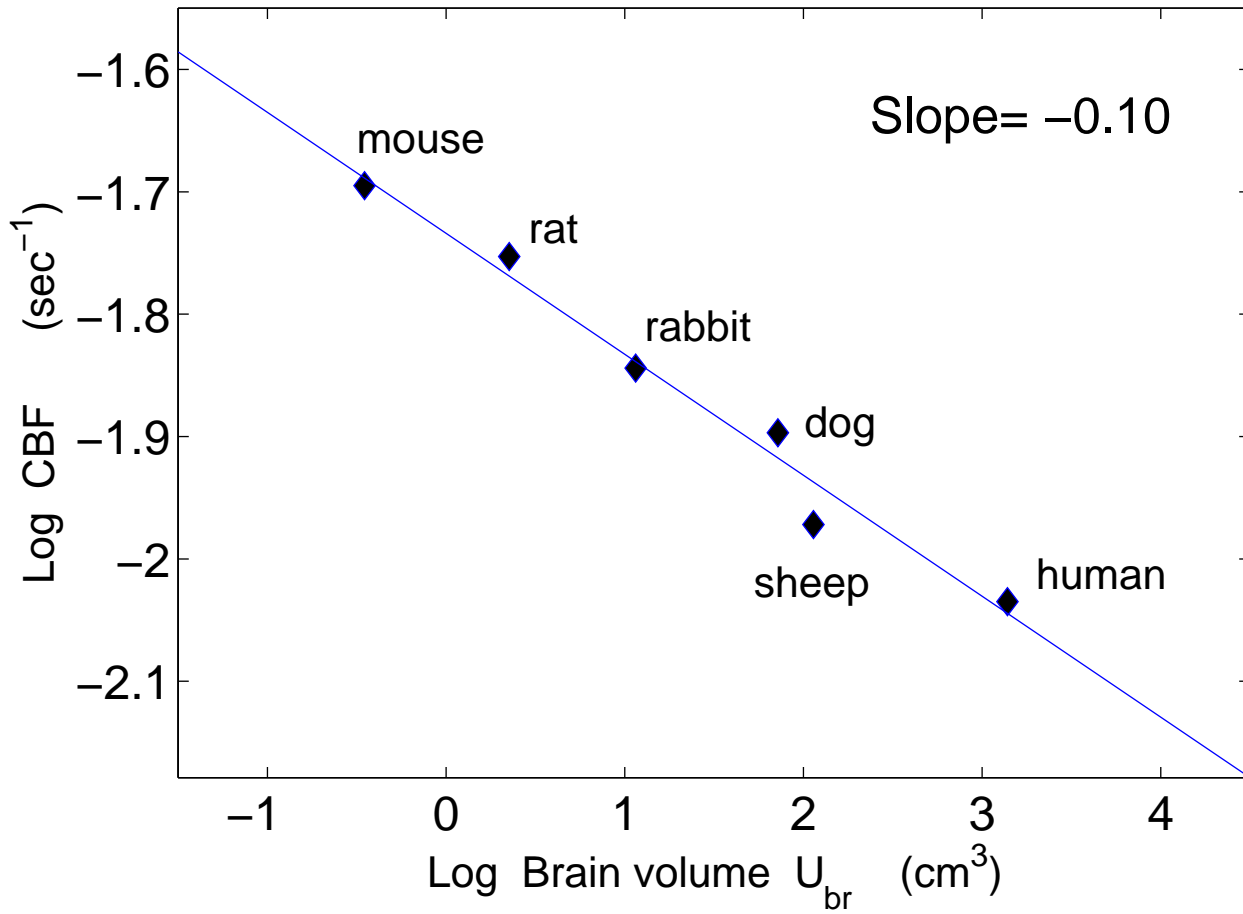


Figure 8A

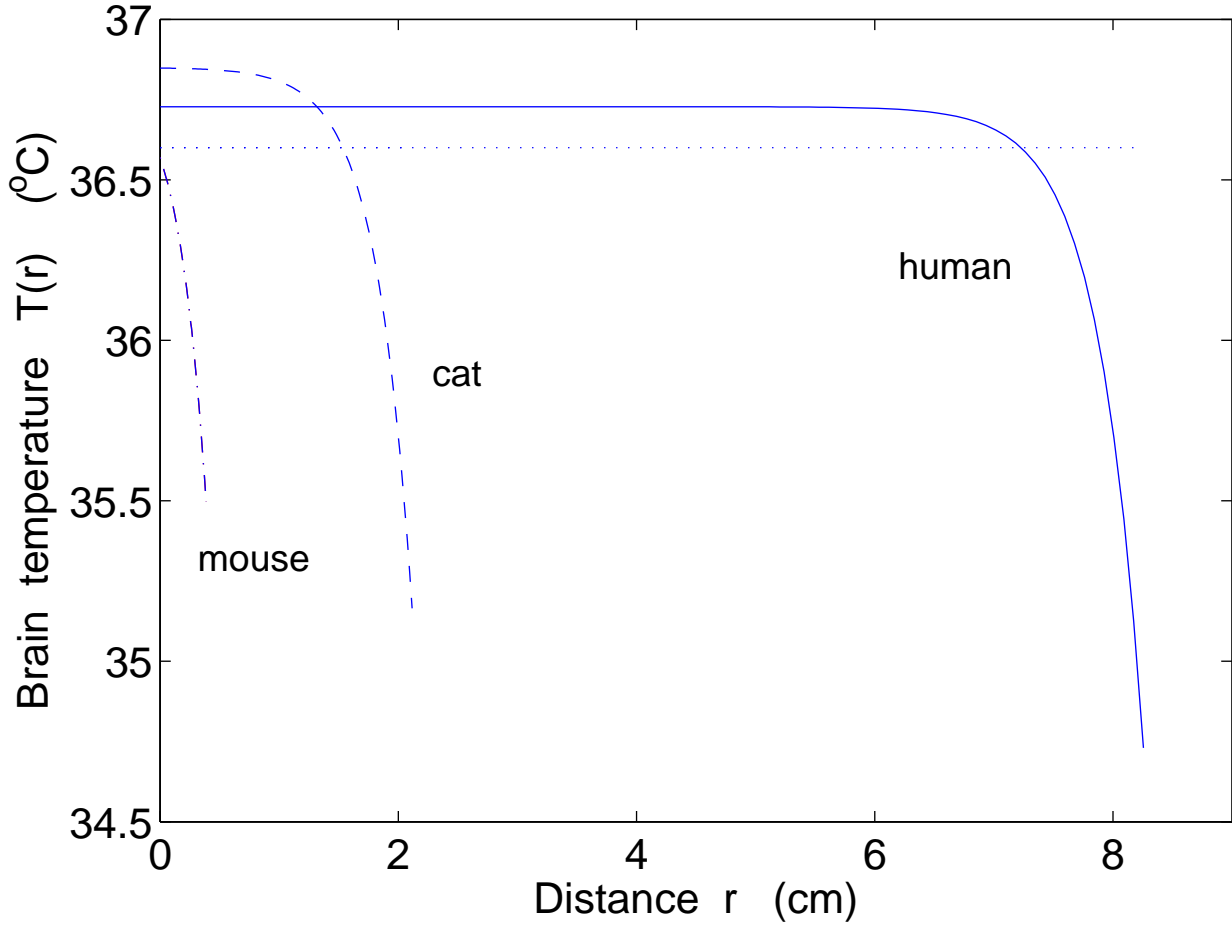


Figure 8B

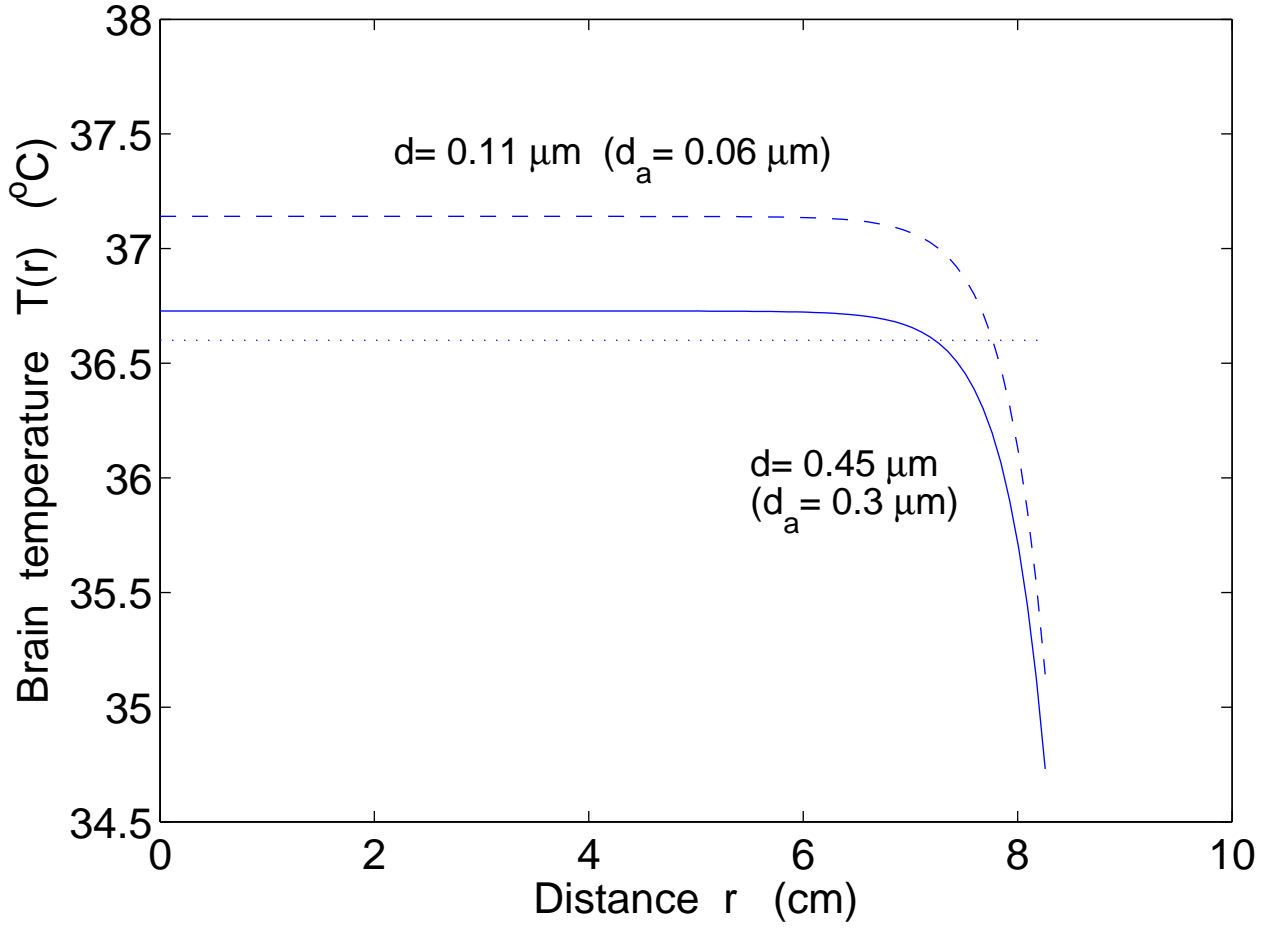


Figure 8C

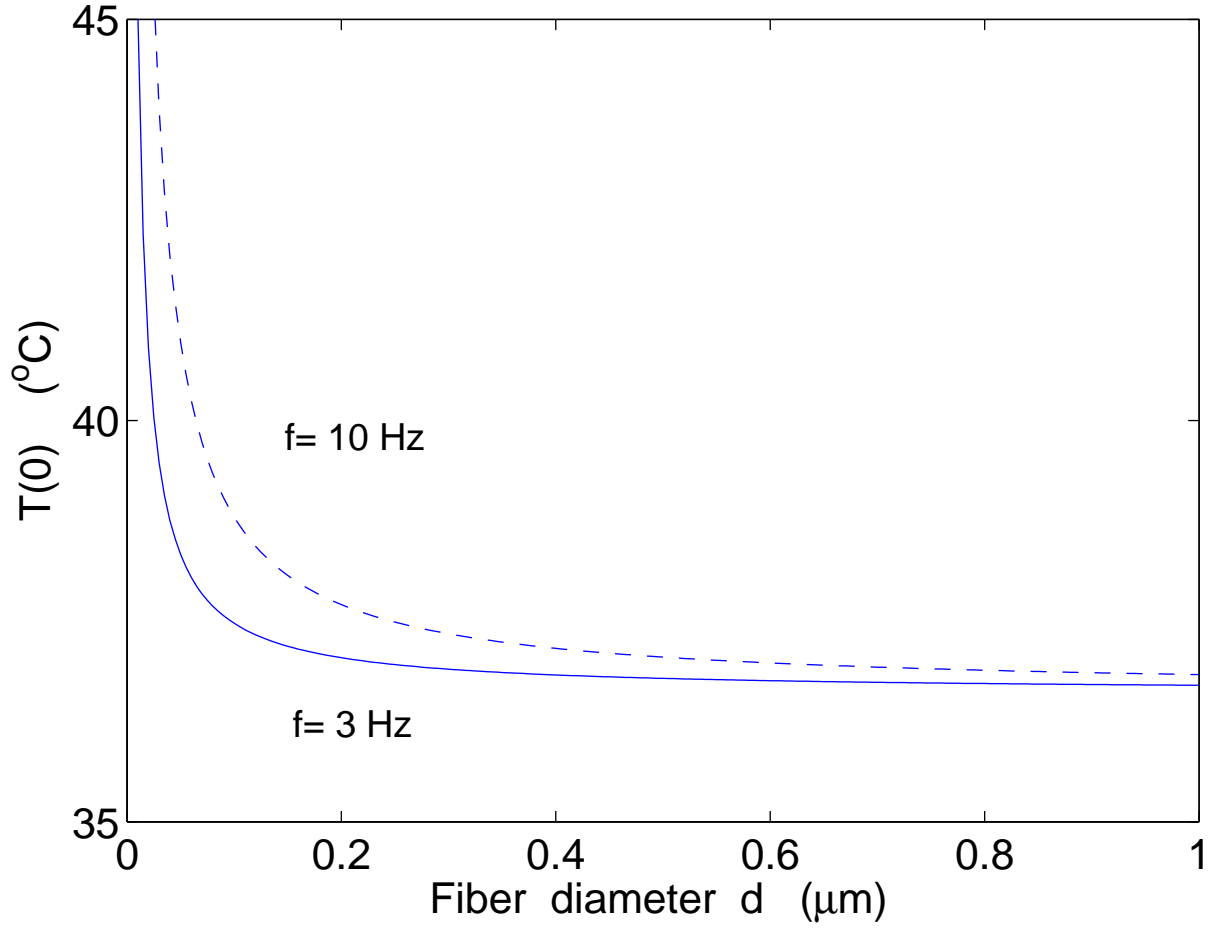


Figure 8D

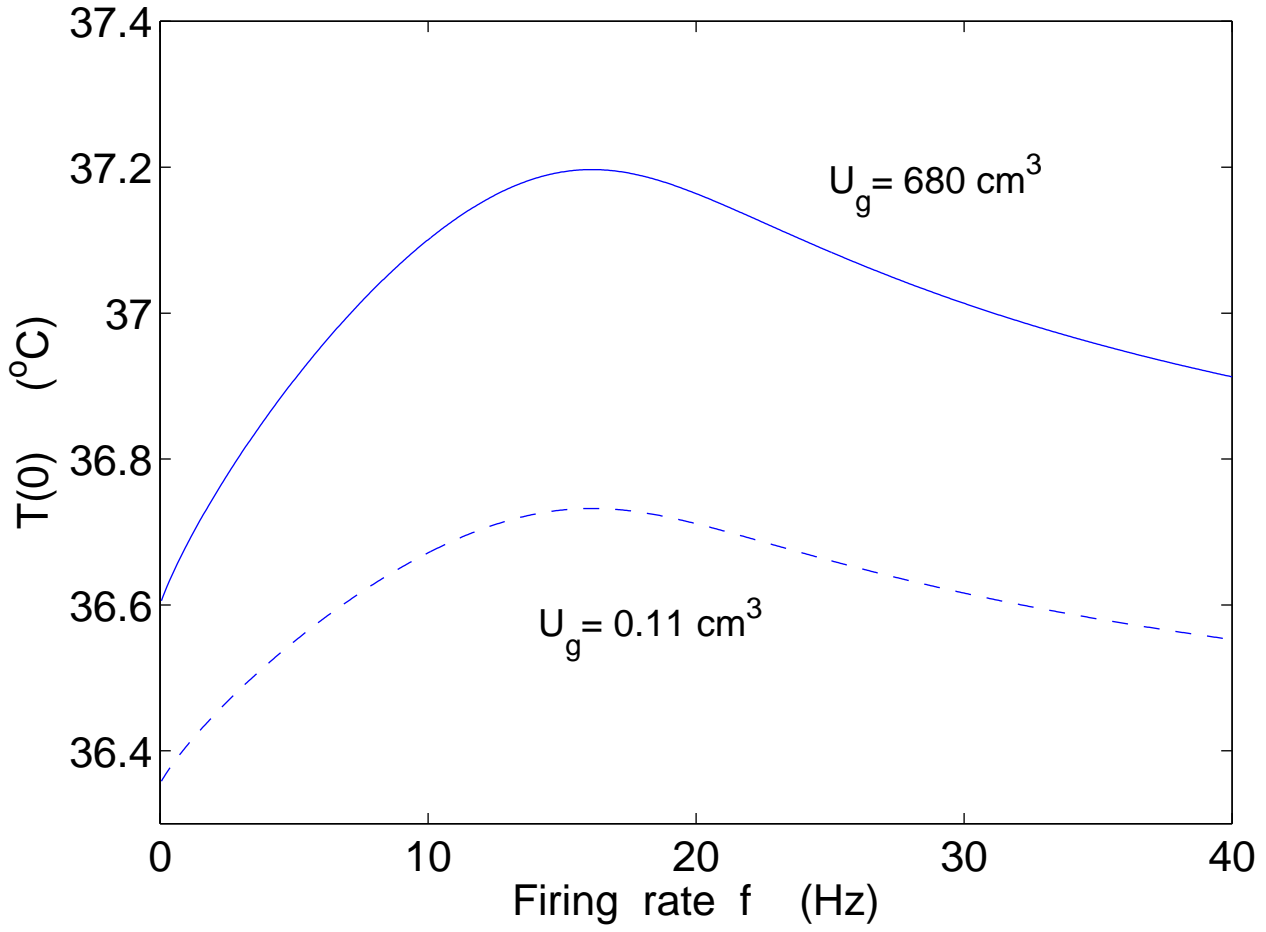


Figure 9A

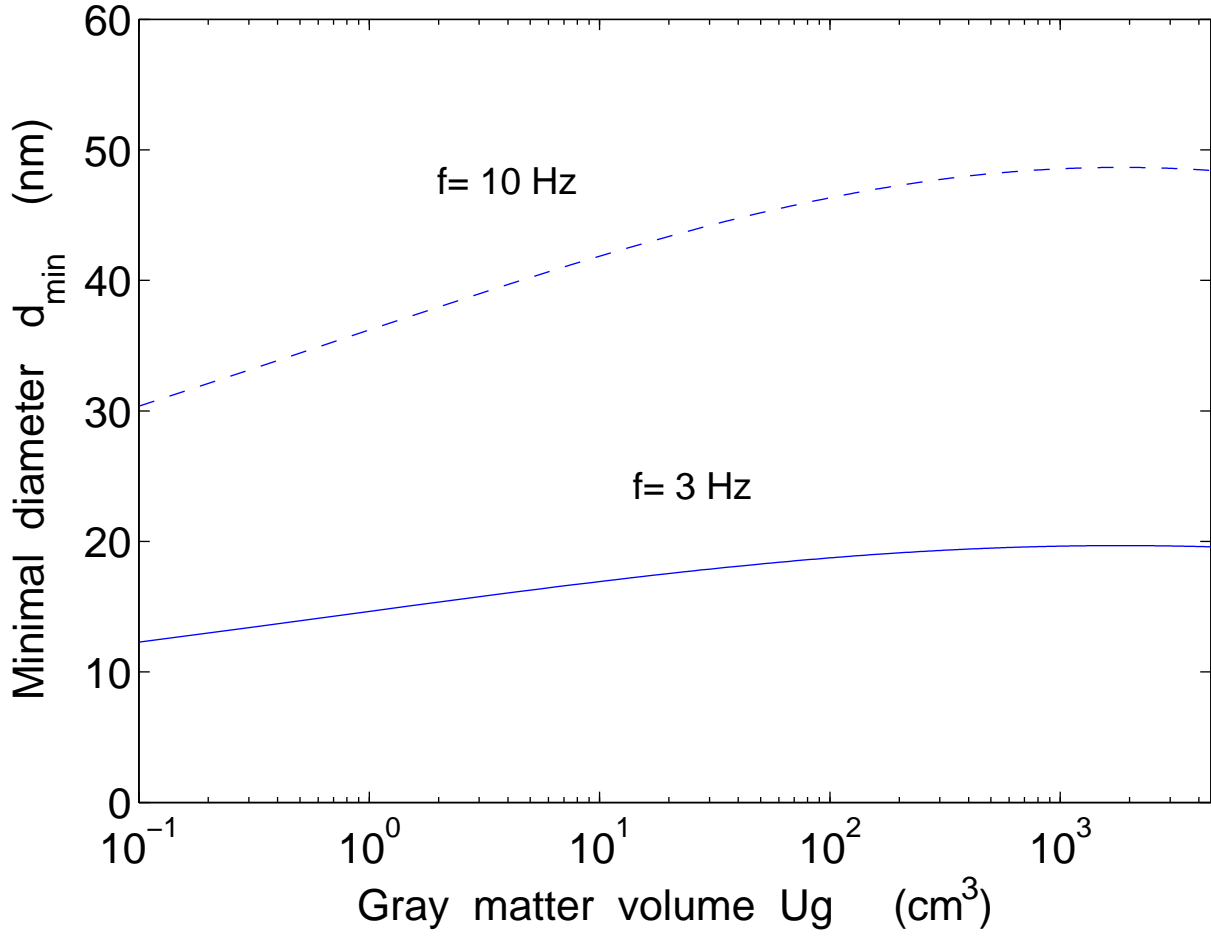


Figure 9B

